Universitetet i Stavanger

FACULTY OF SCIENCE AND TECHNOLOGY

BACHELOR'S THESIS

Study program/specialization: Energy & Petroleum Engineering	Spring semester, 2023 Open access
Author: Vidar Johannes Sandvik	Vidar Johannes Sandvik (Author's signature)
Supervisor(s): Dr. Mahmoud Khalifeh Dr. Reidar Inge Korsnes	
Title of bachelor's thesis: Investigating the Necessity of Standardized In-Situ Testing Procedures for One-Part Granite-based Geopolymers: An Experimental Study of the Influence of Pore Pressure	
Credits: 20 ECTS	
Keywords: Geopolymer plug Downhole conditions Geomechanics Triaxial test	Number of pages: 58 Stavanger, 15th May 2023

Investigating the Necessity of Standardized In-Situ Testing Procedures for One-Part Granite-based Geopolymers: An Experimental Study of the Influence of Pore Pressure

By
Vidar Sandvik

Bachelor's Thesis
Presented to the Faculty of Science and Technology
The University of Stavanger

University of Stavanger
May 2023

Acknowledgment

I want to thank my supervisors, Prof. Mahmoud Khalifeh and Dr. Reidar Inge Korsnes, for all their support during this project. Their guidance, training, patience, and expertise have been deeply appreciated and have encouraged me to perform at my best.

I also acknowledge the Research Council of Norway (RCN) for financing the Centre for Research-based Innovation “SWIPA - Centre for Subsurface Well Integrity, Plugging and Abandonment,” RCN proj. no. 309646, for which the work has been partially carried out.

Lastly, I gratefully acknowledge TotalEnergies, AkerBP, ConocoPhillips and the Research Council of Norway for financially supporting the SafeRock KPN Project (RCN #319014) at the University of Stavanger, Norway.

Abstract

Portland cement has been the primary binder used in well construction due to its availability, affordability, and favorable characteristics. However, alternative options are being explored due to well integrity challenges originating from the chemistry of Portland cement and its environmental impacts due to greenhouse gas emissions during its manufacturing. Geopolymers have emerged as a promising alternative material due to their favorable laboratory testing results and ability to meet most qualifications for barrier materials in NORSOK Standard D-010. As geopolymers move closer to commercialization, standardized testing protocols will be necessary.

In this project, the effect of pore pressure on the mechanical strength and elastic modulus of geopolymers has been researched using a triaxial setup. During this research, 12 geopolymer samples were prepared, where six were tested with pore pressure and the rest without. The tests were performed under three different conditions, where two tests were performed with and two without pore pressure at each condition.

The obtained results show that applying pore pressure impacts the geomechanical properties of the geopolymers. For the hydrostatic phase, the tests performed with pore pressure had linear and repeatable stress versus strain curves that did not change form during the hydrostatic loading phase. During this phase, improved repeatability was observed for the tests performed with pore pressure applied. The repeatability was improved for both the measured strains and the Bulk modulus. Furthermore, the tests performed at 120℃ with applied pore pressure were stronger and had even better repeatability than those performed at 90℃ with applied pore pressure.

In addition, it is worth noting that pore pressure impacts the deviatoric phase. The tests conducted with applied pore pressure exhibited greater repeatability in terms of both the mechanical strength and the shape of the axial stress versus strain curves. The results also suggest that the applied pore pressure may enhance the repeatability of Young's modulus, although further experiments are required to draw a definitive conclusion. It should be noted, however, that pore pressure did not appear to affect Poisson's ratio.

Acronyms

ANN	Artificial neural network
API	American petroleum institute
Al	Aluminium
BOP	Blow out preventer
CO_2	Carbon dioxide
DHSV	Downhole safety valve
E	Young's modulus
GGBFS	Ground granulated blast furnace slag
H_2S	Hydrogen sulfide
JAW-B	Just-add-water–B
KOH	Potassium hydroxide
K	Bulk modulus
LVDT	Linear variable differential transformer
OH^-	Hydroxide
OPC	Ordinary Portland cement
O	Oxygen
PPBD	Paired pressure bidirectional
PRD	Paired rate delivery
P&A	Plug and abandonment
RPM	Rotations per minute
Si	Silicon
σ	Stress
σ_a	Axial stress
σ_h	Hydrostatic stress
ε	Strain
ε_a	Axial strain
ε_r	Radial strain
v	Poisson's ratio

Table of contents

List of figures

List of tables

1 Introduction

Portland cement is the prime material for primary cementing and plug and abandonment (P&A) operations. Primary cementing operations aim to obtain well integrity by creating a hydraulic seal, protecting casing strings against the downhole corrosive environment, and anchoring casing strings. The reason for P&A operations is to obtain permanent barriers, i.e., to restore caprock or its functionality, in the well that isolates both the reservoir and flow zones and to make it safe to abandon the well permanently. In case of well abandonment, an environmental plug (cement plug) will be installed to protect the environment (Kamali et al., 2021; Vrålstad et al., 2019).

It is essential that the cementing material used in primary cement operations and P&A operations obtain well integrity and maintain integrity in an "eternal" time perspective. Some minimum criteria for cementing materials have been made to ensure they meet the abovementioned goals. These criteria differ from country to country, but the criteria used on the Norwegian continental shelf are defined by Norsok Standard D-10 (NORSOK D-010, 2021). These criteria are:

- Long-term integrity (eternal perspective).
- Impermeable.
- Non-shrinking.
- Able to withstand mechanical loads/impacts.
- Resistance to chemicals/substances (H_2S, CO_2, and Hydrocarbons).
- Ensure bonding to steel.
- Not harmful to steel tubulars integrity.

Cement meets some of these criteria but does as well have some significant shortcomings:

- Exposure to CO_2 will cause the cement to degrade, and exposure to H_2S will have a detrimental effect where cement will lose most of its mechanical strength and decrease in weight.
- Cement does not withstand high temperatures over time (Wang et al., 2017).
- Shrinkage can cause micro-annuli, debonding, and radial cracks (Jafariesfad et al., 2017).
- Cement is brittle and has low ductility (Zheng et al., 2022).
- Sensitive towards mud contamination and other parameters related to the cementing job. (Kamali et al., 2020; Khalifeh et al., 2013; Vrålstad et al., 2019).

Due to the weaknesses of cement, the oil and gas industry has been actively looking for alternative solutions to improve its shortcomings or replacing it with new materials. Due to this search, several alternative/emerging materials have surfaced that might replace cement as a superior material. Geopolymers are an emerging material that has shown promising results during laboratory tests. Laboratory tests have shown that geopolymers are superior in many ways to cement and have proved

that geopolymers can possibly be a good cementitious material for the industry. Even though geopolymers look promising, more research is still needed. (Hamie et al., 2022; Khalifeh et al., 2014; Liu et al., 2020; Panchmatia et al., 2020; Salehi et al., 2019; Salehi et al., 2017).

2 Objective

This project is part of a larger effort to determine whether standard rock mechanical protocols adequately describe the mechanical properties of geopolymers or if specific standards are needed. As such, the main objective of this thesis is to investigate the impact of pore pressure on the in-situ mechanical properties of rock-based geopolymers during triaxial testing at various temperatures. By doing so, we hope to gain a deeper understanding of how pore pressure affects the behavior of geopolymers and how this can be accounted for in testing protocols. This will be done by creating 12 geopolymer cores of the same recipe and performing 12 triaxial tests, where half will be with pore pressure, and half will be without. The test data will then be analyzed, and the mechanical properties and elastic modulus will be determined. These data will then be compared to conclude whether the pore pressure affects the properties of granite-based geopolymers.

Furthermore, the thesis will also aim to describe primary cementing, P&A, binding materials, and geo-mechanical properties in an easy-to-understand way. By this, the theory section should be an extended introduction to the thesis with all the critical knowledge needed to understand why geopolymers can be a viable substitute for Portland cement. It should also describe where binding materials are used and which characteristics are important for a binder. Furthermore, the reader should also obtain some knowledge of geomechanics.

Lastly, the thesis will aim to have a detailed methodology section that will make it possible to replicate the experiments. This will be done by providing a mixing procedure and a thorough testing procedure that will make it possible to replicate the experiments. As well as creating samples in the same way as the samples used in this project were created.

3 *Theory section*

3.1 Zonal isolation

During drilling operations, the wellbore will be drilled in sections due to the formation's rapidly increasing pressure and the difference in stability of the formation. Casing strings of different sizes must be installed to make it possible to drill deep enough to reach the reservoir. The first strings are named conductor and surface casing. These strings are cemented to the top and are used as a fundament for the wellhead and the BOP (Blow out preventer). After the surface casing, an intermediate casing will be installed and cemented as long as necessary. As wells vary in depth, several intermediate casings might be installed to reach the depth close to the reservoir. These casings do protect weaker formations and make it possible to drill deeper. The last casing installed will be the production casing. This casing is cemented as long as necessary and is used to reach the reservoir (Liu, 2021, pp. 17-23).

One of the main objectives of the cement pumped between casing and formation is to create a barrier that prevents communication between different zones. This barrier is named primary cementing or zonal isolation and provides several functions. These functions are (Liu, 2021, pp. 3-8):

- Blowout prevention
  The cement between the casing and formation creates a hydraulic seal that acts as a barrier against the reservoir and other potential flow zones. This barrier maintains well integrity and prevents hydrocarbons from traveling along the annular to the surface and creating a potential blowout. The cement does as well anchor the surface casing that is used to mount the wellhead and BOP. In other words, zonal isolation is an essential part of the primary barrier and an important part of the secondary barrier.
- Loss of circulation
  Casings and cement make it safe and possible to drill deep wells through weak formations or formations with other characteristics like high permeability and abnormal pressures.
- Protection of casing
  Cement is also used to protect the casing from the downhole corrosive environment.
- Water protection
  Protecting the groundwater from the well might be necessary if a well is drilled onshore. This task will be done using zonal isolation.

  As seen above, zonal isolation is essential to well construction and obtaining and maintaining well integrity during the drilling process and the well's life. Due to the importance of the tasks performed by zonal isolation, the zonal isolation must perform its job without failures. These

tasks must be performed during the well's entire life, and the zonal isolation might also be a part of the P&A process.

3.2 Plug and abandonment (P&A)

Plug and abandonment of a well is the operation that takes place when there is a need to abandon the well, either temporarily or permanently. There are three types of plug and abandonment operations of a well. In the first case, called suspension, the well control equipment is not removed. There might be different reasons for a suspension, like rough weather, waiting on equipment, working on another well, logistics, etc. But common for all suspensions is that well control equipment maintains the well's integrity. Another type of abandonment is temporary abandonment. This type of abandonment occurs when the well control equipment is removed, and other barriers downhole maintain the well integrity. Temporary abandonment is typically done when there will be a more extended period before re-entry of the well or when the well is planned to be permanently abandoned later. This might, for example, be when a drilling rig is available or when the drilling department has the capacity for a permanent P&A operation. As mentioned, the last P&A operation is permanent P&A. This operation is performed on a well when it has served its purpose as a producing or exploration well, and there is no intention of ever re-entering the well (Khalifeh & Saasen, 2020, pp. 1-4).

When performing a permanent P&A operation, several aspects need to be considered. One of these aspects is the well barriers. During any time of a well's life, one primary barrier envelope and another secondary barrier envelope should always be in the well. This comes from a generally accepted rule that a single failure of a barrier component should not lead to unacceptable consequences. These barrier envelopes can consist of several parts like mechanical plugs, casing, cement, downhole safety valve (DHSV), X-mas tree, and more for temporary P&A operations. But there are some considerations for barriers used for Permanent P&A due to the eternal time perspective. These considerations relate to which materials can be used as a material for permanent P&A. An example is that mechanical plugs can't be used as a permanent barrier due to long-term durability concerns (Khalifeh & Saasen, 2020, pp. 6-12, 16).

For permanent P&A applications, some criteria have been set for the cementitious materials used to create permanent plugs and barriers in wells. These criteria are written in the Norsok D-010 standard and listed earlier in this text (NORSOK D-010, 2021). All barriers used for permanent abandonment/ barriers should fulfil these previously mentioned criteria to ensure that well integrity will be kept in an eternal perspective (Khalifeh & Saasen, 2020, pp. 97-137).

Another aspect to consider with permanent P&A is the placement of plugs to create a reliable barrier. In both Norway and UK, some standards describe the acceptable placement of permanent plugs. These standards divide a permanent P&A operation into 3 phases, the first being reservoir abandonment. In

this phase, two separate plugs should be placed towards the reservoir to act as primary and backup barriers. The second phase, intermediate abandonment, requires the placement of two separate permanent plugs to create primary and backup barriers for potential flow zones in the overburden. There should also be placed a surface plug under the seabed. This plug protects the environment from contamination from residues of fluids from the abandoned well. Lastly, the third phase is to remove the wellhead and conductor (Vrålstad et al., 2019).

3.3 Cementitious materials

3.3.1 Ordinary Portland cement (OPC)

Portland cement was invented in 1824 by the inventor Joseph Aspdin. Since Joseph Aspdin thought the final hardened product resembled a Portland stone, he chose to name the product Portland cement. Simply put, this product is produced by heating/burning a mixture of limestone and clay in a cement kiln to 1450˚C. The outcome of this process is cement clinker balls that are created when the mix cools down. These balls are aged in storage before being grounded to cement powder. Various ingredients will then be added to the cement powder to give the Portland cement the desired properties (Mitchell & Miska, 2010, pp. 139-140).

Since the beginning of well construction, Portland cement has been the most used binding material for both primary cementing and P&A operations. Portland cement was chosen for well cementing because of the lack of other alternatives and the availability of Portland cement. Despite the lack of competition, Portland cement was as well-chosen without any qualification program. The use started with neat Portland cement, but during the decades of development, several additives have been added to Portland cement, and several classes and types of Portland cement have been developed. Developing new types of Portland cement was necessary to meet the industry's needs when wells were drilled deeper and became more complex (Vrålstad et al., 2019).

Even though Portland cement has many good attributes as a binder in well construction and for P&A, there are shortcomings that are of great concern. These shortcomings are that Portland cement is brittle, has low ductility, and does not withstand high temperatures and corrosive environments over time. It might also be issues related to forces from well operations, poor mud removal, and shrinkage. Even though much research and development have been done in this field to improve Portland cement, shortcomings still exist, as the primary root is cement chemistry. Moreover, the production of Portland cement contributes to greenhouse gas emissions and is related to global warming. The shortcomings of cement have made the industry start looking for new materials for a binder in well construction. Currently, there are several alternative/emerging alternatives with different characteristics. One of these emerging alternatives is geopolymers (Kamali et al., 2021; Khalifeh, 2016; Vrålstad et al., 2019).

3.3.2 Geopolymers

Geopolymers are inorganic cementitious binders first introduced by the scientist and inventor Joseph Davidovits in 1978. Davidovits had developed an alkali-activation of metakaolin and patented it with the name geopolymer. Since then, there has been much development in the field, and geopolymers have been developed using many different aluminosilicate source materials. These aluminosilicate materials combined with various additives can help create geopolymers with diverse characteristics. These characteristics will be aimed toward the intended use of the geopolymers. For example, the wanted characteristics for geopolymers intended for well cementing differ from those used for construction purposes (Awoyera et al., 2020; Khalifeh et al., 2019; Pacheco-Torgal et al., 2008).

Geopolymer synthesis is a process consisting of three main steps. The first step is the dissolution of the aluminosilicate source. This happens because of the presence of Hydroxide (OH^-) in the hardener that dissolves the aluminium and silicate-rich precursor, which are amorphous. As a result of the dissolution Al-O-Al, Si-O-Si, and Si-O-Al bonds are formed, and we end up with silanol groups. The second step is the transportation/orientation and oligomerization step. During this step, the dissolved products change orientation and create monomers that react with each other and form different structures. These structures will be of various shapes and forms but are known as oligomers. The last step is referred to as geopolymerization or polycondensation. In this step, the oligomers interact and form three-dimensional networks. These aluminium silicate networks are known as geopolymers (Khalifeh et al., 2019; Pacheco-Torgal et al., 2008).

It has been found that geopolymers do have attractive properties from laboratory testing that can make them a possible substitute for Portland cement. To be able to substitute Portland cement for both P&A and zonal isolation applications, there are some characteristics that the binder must possess. Such properties include but are not limited to: providing long-term integrity with an eternal perspective, being impermeable or having very low permeability, non-shrinking, ductile, resistant to chemicals/substances, ensure bonding to steel, not harmful to steel tubulars integrity (NORSOK D-010, 2021).

Geopolymers have been tested to see if they have these characteristics. Geopolymers exposed to crude oil and CO_2 did show promising results, but for H_2S exposure, the sample were partly deteriorated (Khalifeh et al., 2017). Research shows that a geopolymer's ability to bond to steal depends on how much hardener there is in the mix. Other promising results are that geopolymers have low permeability, low chemical shrinkage, can withstand high temperatures, and are ductile compared to Portland cement. These results have been achieved only through laboratory testing as geopolymers are still at an early stage, so it is necessary with field testing as well (Khalifeh et al., 2019; Khalifeh et al., 2017). One issue concerning field testing has been the pumpability of geopolymers. There has been achieved control of pumpability by using admixtures, but this task is sensitive and time-consuming. Another solution to expedite the developments on controlling pumpability of geopolymers is creating and implementing

computer programs, e.g., decision tree or ANN (Artificial neural network), that can predict the trend of pumpability or setting time. This is in the early stage and requires additional research (Hamie et al., 2022; Ling et al., 2021).

3.3.3 Geopolymers versus Portland cement

As geopolymers are an emerging alternative to substitute Portland cement, there will be a short comparison between some key characteristics between Portland cement and geopolymers here (van Oort et al., 2019).

- Compressive load and strain
  Portland cement will be able to reach a higher compressive strength than geopolymers, and while doing so, the Portland cement will also be strained less than the geopolymers. When reaching the failing point, the Portland cement will have a distinct failure point with a clear peak. Geopolymers will also reach a failing point, but not as distinct as Portland cement. These characteristics describe geopolymers as a more ductile material than Portland cement but also weaker. But for well construction, it is a desired characteristic that the material is ductile and not brittle as the Portland cement is. This is due to diverse downhole environments with pressure fluctuations due to well operations.
- Healing ability
  One important aspect of a binder used as a barrier element is its ability to heal if cracks are formed. There has not been any research showing that Portland cement can heal itself in wells. On the other side, there have been examples of self-healing of cracks reported and observed in geopolymers. This is a good characteristic for geopolymers but still needs more research.
- Bonding
  Laboratory experiments show that geopolymers bond with a factor 2.5-3 higher than Portland cement for shear-bond between pipe and binder. This favors the geopolymers as it is desired to have as high bond strength as possible to keep both binder and casing in place.
- Shrinkage
  Both Portland cement and geopolymers shrink, which is a problem as a binder. Shrinkage can cause several issues in a well. According to (van Oort et al., 2019), the shrinkage for Portland cement and geopolymers are similar, but other research shows that geopolymers have low shrinkage.
- Contamination
  Even minor contaminations of Portland cement can have quite a significant impact on its performance. It can affect its strength and rheological characteristics making it hard to create and pump. Compared to cement, geopolymers have been showing more resistance against contamination. Geopolymers also show the opposite viscosity behavior compared to Portland cement. The viscosity of geopolymers is reduced instead of increased when contaminated.
- Corrosive environment
  Portland cement cannot withstand the corrosive downhole environment over time, it will be degraded by CO_2, and H_2S will deteriorate it. Compared to geopolymers, geopolymers are not affected by CO_2 but will be partly deteriorated by H_2S.

In conclusion to the comparison, geopolymers have many good characteristics compared to Portland cement, making it a good fit as a substitute barrier material. Even though geopolymers look promising, further research is still needed before geopolymers can be qualified as a barrier material for primary cementing and P&A applications. In addition to the comparison of characteristics, it is worth mentioning that geopolymers are also a green alternative to replace Portland cement.

3.4 Geomechanics

3.4.1 Triaxial test

A triaxial test is a common way to determine a sample's mechanical properties and elastic modulus. The test is usually performed on a cylindrical sample. It is possible to apply stresses to the sample from all directions during the test, including pore pressure. The stresses are applied by having a confining pressure around the sample, a deviatoric load in the axial direction, and a pore pressure from an injection of fluid through the sample. A triaxial test can also be used to obtain other properties like creep, stress relaxation, permeability, and more (Lade, 2016, pp. 37-40). During the experiments performed in this thesis, triaxial tests will be used to determine the sample's mechanical properties and the elastic modulus.

3.4.2 Stress

Stress describes the distribution of a force on a defined area. This can be described by a pole standing on a level surface with a load added on top. Then the stress applied on the surface from to the pole can be calculated by the definition of the stress formula:

$$\sigma = \frac{F}{\mathrm{A}} \tag{2.1}$$

where:

σ = Stress

F = Force

A = Area

As stress is a function of an area and applied force, the stress through the pole will vary in magnitude if the area changes and the force coming from the load is constant. A thinner part of the pole will be subjected to a higher magnitude of stress, and a thicker part will be subjected to a smaller magnitude of stress. Stress will be applied to the samples in these experiments by using hydraulic pressure. Both axial and radial stress will be applied by pumping a fluid into a constraint area to build up pressure. In the case of radial stress, the pressure will act directly onto the sample. For the axial stress, pressure will act on top of a piston that will transfer the axial stress to the sample (Fjær et al., 2008a, pp. 1-3).

During the experiments, there will also be applied a third pressure. This pressure will be applied by injecting a fluid into the sample pores and pressurizing it. The pressure from the pressurized pore fluid will act opposite to the externally applied pressure and lower the effective stress the sample is subjected to. To be able to calculate the effective stress that is acting on a sample with both external and pore pressures applied, the formula for effective stresses will be used:

$$\sigma' = \sigma - \alpha P_f \tag{2.2}$$

where:

σ' = Effective Stress

σ = External stress

α = Biot coefficient

P_f = Pore pressure

During these experiments, the Biot coefficient will be set to 1. The reason for this is that the Biot coefficient for geopolymers is unknown and that the Biot coefficient will have a small effect in the effective stress calculation since the applied pore pressure will only be 0.7 MPa. The effective stress equation will be used to calculate stress when applying pore pressure (Fjær et al., 2008a, pp. 32-35; 2008c, pp. 114-117)

3.4.3 Strain

Strain defines the deformation happening to a sample when subjected to an external force. When a sample is subjected to axial stress, the axial length change will be named axial strain. The same applies to radial stress. When a sample is subjected to radial stress, the change in diameter will be called radial strain. Strain is defined by the formula:

$$\varepsilon = \frac{L - L\prime}{\mathrm{L}} = \frac{\Delta L}{L} \tag{2.3}$$

where:

ε = strain [%]

L = Length before stress

L' = Length after stress

ΔL = strain

Since the sign definition of stresses is positive for compressive stresses, the sign definition for strain is set to be compatible with the signs for stresses. This results in a positive strain for contraction and a negative strain for elongation (Fjær et al., 2008a, pp. 13-15).

3.4.4 Elastic modulus (Young's modulus, Bulk Modulus, And Poisons Ratio)

A core subjected to a deviatoric load will first be compressed/deformed elastically before it becomes plastically deformed. Young's modulus is measured during elastic compression and is described by the formula:

$$E = \frac{\sigma_a}{\varepsilon_a} \tag{2.4}$$

Where:

E = Young's modulus

σ_a = Axial stress

ε_a = Axial strain

Young's modulus describes the elasticity of the sample in the elastic region and can be used to say something about the ductility of the core being tested. During my experiments, Young's modulus will be measured in the deviatoric phase by deciding on a set interval at the beginning of the elastic phase. The measurement will be done by making a trendline over the selected interval. The line's rate of increase will be the measured Young's modulus (Fjær et al., 2008a, p. 20; Zhang, 2019, pp. 60-63).

Poisson's ratio measures how much a sample deforms in the radial direction compared to the contraction in the axial direction. The modulus is given by the formula:

$$v = -\frac{\Delta \varepsilon_r}{\Delta \varepsilon_a} \tag{2.5}$$

where:

v = Poisson's ratio

$\Delta \varepsilon_r$ = Δ Radial strain

$\Delta \varepsilon_a$ = Δ Axial strain

During the experiments, the Poisson's ratio will be measured in the same set interval in which Young's modulus is measured. (Fjær et al., 2008a, p. 20).

The Bulk modulus is described by the volumetric strain happening to a core subjected to a hydrostatic load. In other words, it measures the compressibility of a core while being exposed to a hydrostatic load. This could be an indication of how dense the structure of the tested specimen is. The Bulk modulus is described by the formula:

$$K = \frac{\sigma_h}{\varepsilon_v} \tag{2.6}$$

where:

K = Bulk modulus

σ_h = Hydrostatic stress

ε_v = Volumetric strain

During the experiments, the Bulk modulus will be determined during the hydrostatic phase in two ways. The first way will be to take the average rate of increase over the entire hydrostatic loading. The second way will be by determining a set interval where the Bulk modulus will be defined as the rate of increase of a trendline created over the decided interval (Fjær et al., 2008a, p. 21).

3.4.5 Failure mechanics

Failure of a core is defined as when a core loses its shape permanently, and the possibility to withstand stress is reduced. In the experiments, the failure of the core will happen in a triaxial cell with a defined

confining pressure surrounding it. Due to this testing mode, the failures observed will be shear failures. A shear failure happens when the shear stress is too high for the core to withstand. What happens is that there will be a place where two planes move opposite of each other, and the sample "shears" (Fjær et al., 2008b, pp. 55-61).

Before the sample reaches the shear failure, it will undergo the deformation stages. Firstly, we have the elastic stage. In this stage, the core will deform while being subjected to stresses, but it will return to its initial shape with minor permanent deformation when the stress is removed. The yield point is the maximum that the core theoretically can be deformed in the elastic stage without any permanent deformation. If the sample is applied stress after reaching the yield point, the core will deform permanently. When the core starts to get permanently deformed, it moves into the second deformation stage, the ductile region. The ductile region is the region where the core deforms permanently but still can maintain stresses. This region can vary in length, affected by the elasticity of the core being tested. For a brittle material like Portland cement, the ductile region will be short. But the ductile region can be long for more ductile materials like geopolymers. Lastly, when the core loses its ability to withstand stresses, it enters the brittle region. A rapid loss of strength and failure characterizes this region. In our case, the failure will be a shear failure (Fjær et al., 2008b, pp. 55-61).

4 Methodology and experimental procedure

This chapter will describe the preparation of the JAW-B (just-add-water-B) geopolymer samples from mixing to curing. It will also contain a detailed procedure for performing a triaxial test. It is intended that a person with some previous laboratory experience should be able to replicate these experiments.

4.1 Equipment used for the preparation of the JAW-B samples

Different equipments were used for mixing and curing during the preparations of the geopolymer samples. Below, the main equipments will be described in detail. Otherwise, several minor tools were used. Some examples are scale, funnels, cups, pipettes, spatula, mixing bucket, spoons, and more.

4.1.1 Ofite model 20 constant speed blender

Figure 1: Ofite model 20 constant speed blender

The constant-speed blender was used to mix the dry and liquid components, Figure 1. The automatic program following the API specifications was used when components were mixed. This program

consisted of two phases, where the first phase was mixing at 4000 RPM for 15 seconds. In the first phase, the dry components were added evenly to the liquid with the help of a funnel. After the first 15 seconds had passed, the second phase started automatically. The second phase was mixing at 12000 RPM and lasting 35 seconds. The second phase is to ensure that all the components get properly mixed.

4.1.2 Ofite model 60 atmospheric consistometer

Figure 2: Ofite model 60 atmospheric consistometer

Before the curing procedure started, the last step was to condition the slurry for 30 minutes at 30 degrees. For this task, the Ofite consistometer was used, Figure 2. The consistometer is made for conditioning cement according to API specifications. Conditioning means simulating the bottom hole conditions that the slurry will encounter when being pumped in place. During the experiments, the consistometer was only used for conditioning, but the consistometer can also be used to measure the slurry's consistency.

4.1.3 Equipment for curing samples

The equipment used for curing the samples includes curing molds, an autoclave cell, a heating cabinet, and a pump. There will be a quick overview of the equipment collectively since the different pieces of equipment work together to perform the curing process.

- Curing molds

  The curing molds made it possible to make samples the same shape for every test, Figure 3. The curing molds consist of a split cylinder, a bottom lid, a top lid, and two hose clamps. When the mold is assembled, the bottom lid should be installed, and then the split should be closed with the help of hose clamps. Before installing the top lid, the slurry should be poured into the mold. After the slurry was poured in and the top lid was installed, the curing mold was ready to be placed in the autoclave cell. When the curing is complete, the hose clamps are loosened, and the split in the cylinder is reopened. The reopening should make extracting the cured sample from the mold easy.

Figure 3: To the left and middle are pictures of a curing mold, and to the right is a picture of an autoclave cell

- Autoclave cell

  The autoclave cell was used to apply pressure around the samples, Figure 3. First, the autoclave cell was filled with water, and then the molds were placed inside the cell.

- Heating cabinet

  The samples inside the autoclave cell were cured in a heating cabinet at 90˚C and 2000 psi for 7 days.

- VP-series Pump from Vindum engineering

  Lastly, there was a pump placed on the outside of the heating cabinet. The pump had liners going inside the cabinet that was connected to the autoclave cell, and the pump was used to apply 2000 psi.

4.2 Preparation of JAW-B geopolymer samples

4.2.1 Materials

When creating the JAW-B geopolymer samples, there are two main components. These main components are the precursors and the hardener. The precursors are the raw materials that the hardener should break down. The precursors are characterized of being silicate and aluminium-rich. In this project, the silicate and aluminium-rich precursors used are a blend of GR (granite), GGBFS (ground granulated blast furnace slag), and micro-silica. The hardener used in this project is potassium silicate. Since a hardener used for creating geopolymers needs to be very reactive to react with the precursors, an alkali activator containing alkali metals is used. Due to these metals being located in the first group in the periodic table, they only have one electron in the outer shells and will easily react to fulfil the octet rule (Khale & Chaudhary, 2007).

In the JAW-B geopolymer, the precursors and hardener are dry components that can be mixed in a dry phase without reacting. The reaction starts when water is added to the dry mix. In the JAW-B mix, a shot of KOH will also be added. The added KOH will increase the alkali concentration to what is needed for the reaction to go as supposed. In the JAW-B recipe, the mixing sequence will be to add KOH to water before adding it to the premixed dry phase.

4.2.2 Jaw-B geopolymer ingredients

- Dry components:
    - GR (Granite)
    - GGBFS (Ground granulated blast furnace slag)
    - Micro silica
    - Potassium silicate
- Liquid components:
    - Distilled water
    - Shot accelerator KOH 12 M

4.2.3 Mixing and conditioning procedure

It is important to follow some guidelines while working in laboratories. The minimum requirement for PPE (personal protective equipment) while working in laboratories should always at least be to wear a lab coat and safety glasses. For mixing the JAW-B geopolymer, there are some additional requirements to follow. Mixing dry components should always be done in a fume hood while wearing an appropriate dust mask and chemical gloves.

1. Ensure all necessary mixing equipment is available, clean, dry, and ready to use before mixing.

2. Weigh up all the dry components while placing them into a mixing bucket. Put the lid onto the bucket when all the dry components are placed in it. Shake the bucket firmly for at least a minute to properly mix the dry components.
3. Move the mixed dry components from the bucket to a container.
4. Weigh up the liquid components into the mixing cup belonging to the Ofite blender.
5. Place the mixing cup into the Ofite blender and put a funnel on top of it. Start the API mixing program. During the first 15 seconds of the program, the dry components should be evenly added. During the last 35 seconds, the components should be properly mixed.
6. After mixing, the mix should be transferred to a conditioning cup and placed into the Ofite consistometer.
7. The mix should be conditioned for 30 minutes at 30˚C.

4.2.4 Curing procedure

1. Check that all necessary equipment for curing the samples is available and in good condition.
2. Prepare the curing molds. The molds should be assembled with a bottom lid and hose clamps. All surfaces that will be in contact with the slurry must be lubricated with silicone grease to prevent the geopolymer samples from bonding to the molds.
3. The autoclave cell should be filled with water at approximately 30˚C.
4. Fill the curing molds with geopolymer slurry to 6-8 mm below the top edge and add a layer with distilled water on top of the slurry. Afterward, add the top lids to the molds.
5. Drop the curing molds into the autoclave cell. Assemble the Autoclave cell.
6. Move the autoclave cell into a heating cabinet set to 90˚C and connect a pressure liner to the autoclave cell.
7. Increase the pressure in the autoclave cell to 2000 psi and let the samples cure for approximately 7 days before extracting the samples. While curing, the pump should be placed in a constant pressure mode to keep the pressure constant.
8. Disassemble the autoclave cell and curing molds when the samples are cured. Then extract the sample and keep it in water until the start of the triaxial testing procedure.

4.3 Equipment used for testing the JAW-B samples

4.3.1 Experimental setup

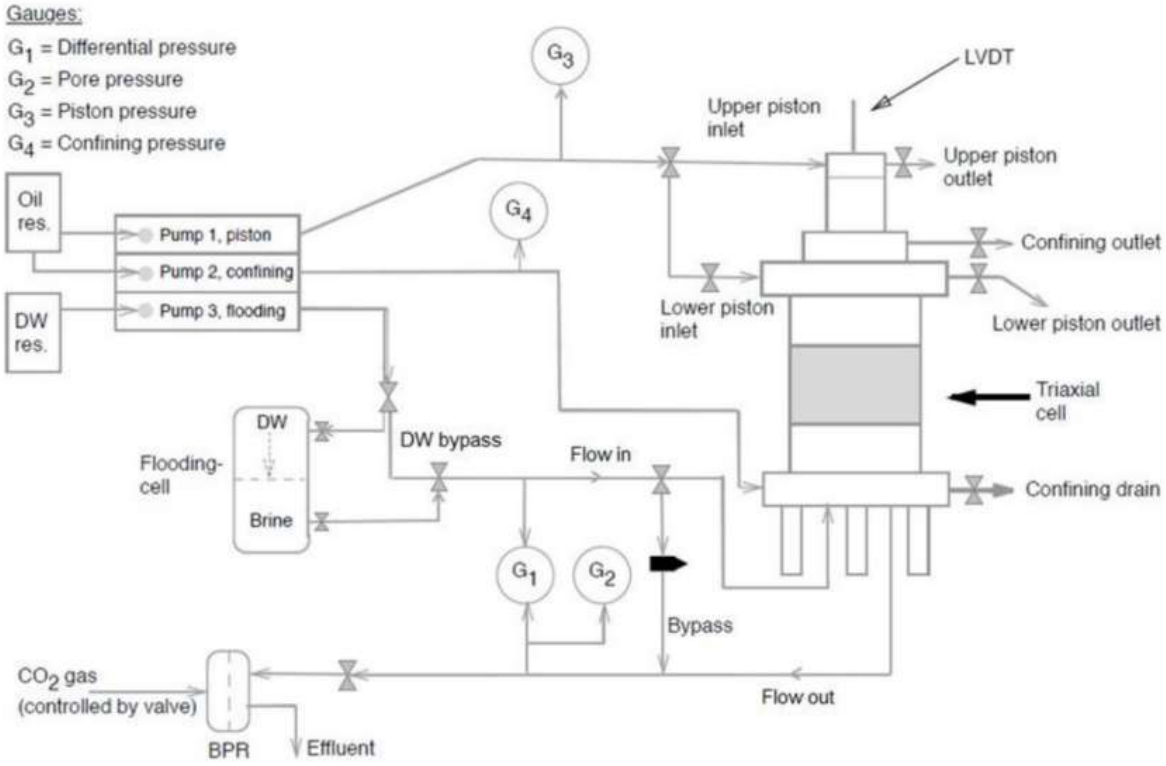

Figure 4: Experimental setup for a triaxial test with flooding (Nermoen et al., 2016)

The experimental setup used during the triaxial tests is illustrated in the sketch in Figure 4. It contains 3 pumps, 1 triaxial cell, and a back pressure regulator that will be described in detail later. Furthermore, the flooding cell has been bypassed in these experiments since all the tests performed with pore pressure have been performed using distilled water.

4.3.2 Cutting and Grinding machine

Figure 5: Cutting machine from Discotom to the left and grinding machine from Baldor to the right

After the cores were extracted from curing molds, they were around 85 mm long. The cutting machine was used to cut the length of the cores down to the pre-determined length. After the cores were cut to the appropriate length, the grinding machine was used to make the cores end-facies parallel, Figure 5.

4.3.3 Triaxial test cell

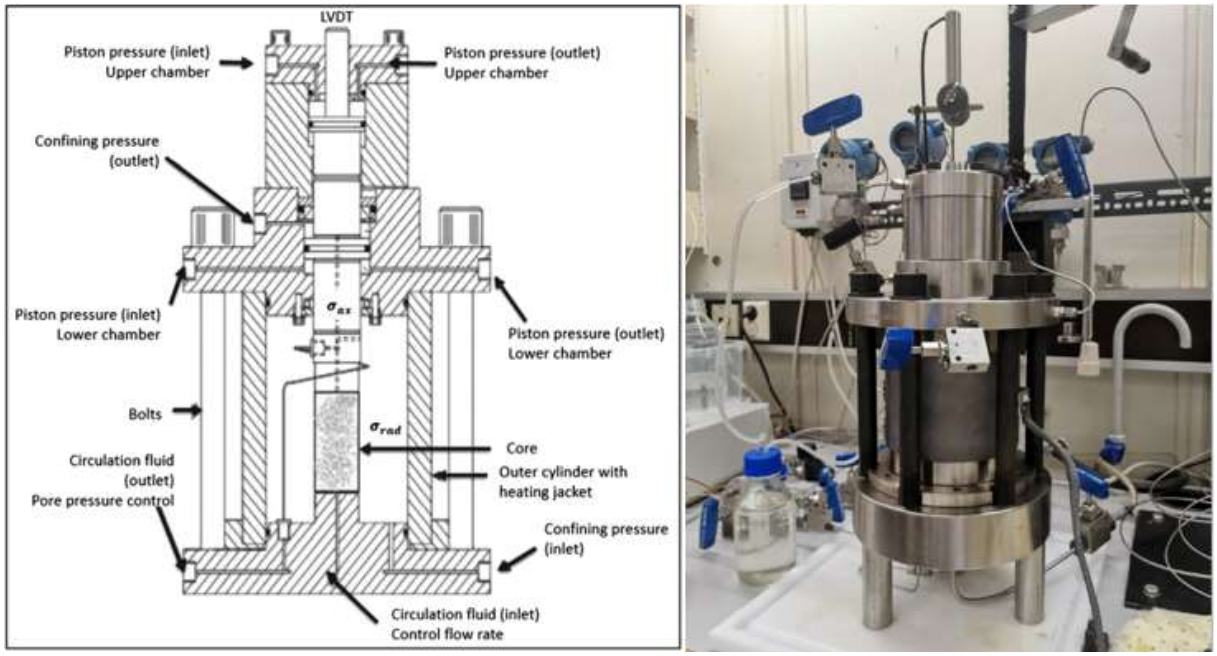

Figure 6: Drawing of the triaxial cell used during my experiments to the left (Nermoen et al., 2015) and a picture of the cell used to the right

The triaxial cell is built up to allow the possibility of simultaneously applying confining, axial, and pore pressure, and at the same time control the temperature and measure axial and radial strain. This allows for experimental studies of geopolymer sample's geomechanical behavior at stresses and temperatures it will be subjected to when used as a binding material in wells. The application used for this thesis is to apply different stresses with and without pore pressure at a set temperature to see what effect the pore pressure has on the mechanical properties and elastic modulus of the samples.

Several stresses must be applied to perform the mechanical tests with the cell. The confining pressure is applied by pumping mineral oil through the confining pressure inlet port until the desired pressure is reached and is removed by bleeding of mineral oil through the confining pressure outlet port, Figure 6. The axial stress is applied by pumping mineral oil into the upper chamber piston pressure inlet port to move the piston down to the core and apply stress. To remove axial stress, the pressure is bled off from the upper chamber piston pressure outlet port. Furthermore, pore pressure is usually applied by flooding a liquid through the core and toward the back pressure regulator. A shrinking sleeve covers the core to separate the confining pressure from the pore pressure. The shrinking sleeve is melted tight around the core and the metal pistons below and above the core. In this project, the pore pressure will be kept constant at 0.7 MPa using a gas-regulated back pressure regulator. Lastly, the temperature is applied by a heating jacket mounted onto the confining chamber. The heating jacket is controlled by an Omron control box that keeps the temperature constant after it has reached the defined temperature with the help of a PT-100 temperature sensor placed inside the confining chamber.

Data from the pumps and measurement devices are continuously collected while performing the triaxial test. LabVIEW is the program used throughout the project to log all the measured data: pressures, flow rates, strain measurement, and other parameters. During the experiments, LabVIEW was also an important tool used to view the abovementioned parameters live and to compare them to each other while testing. An LVDT (linear variable differential transformer) mounted on top of the cell, which measures the movement of the piston, is used to determine the axial strain. An extensometer with a chain around the core measures the change in diameter of the core using an LVDT. That measurement is used to determine the radial strain of the core.

4.3.4 Pumps

Figure 7: Quizix pumpworks software to the left and operating modes to the right

Two Quizix QX pumps were used for applying axial and confining stress during the triaxial tests. These pumps were controlled by the Quizix computer software program. With the help of this software program, one could control what the pumps were doing in detail, Figure 7. The pump operations used during these experiments are described as follows:

1 Pump program 6 (PRD-paired rate delivery)

This mode was used to deliver a constant rate of a fluid. The program was used primarily for flushing liners, increasing confining pressures, and positioning the piston on top of the core.

2 Pump program 12 (PPBD-paired pressure bidirectional)

This program was used to keep the set pressure constant and to perform ramping operations. Ramping operations was used to perform the increase of pressure both for the hydrostatic and deviatoric phase. The ramping operations made it possible to increase pressure from start to target with a predefined rate.

One Gilson pump was used to apply pore pressure. The Gilson pump was controlled directly in the LabVIEW interface and was used only to deliver a fixed rate of distilled water. A back pressure regulator was used to increase/ keep the pore pressure constant at the defined pressure.

4.4 Experimental procedure for a triaxial test with and without pore pressure

4.4.1 Preparation of the core

1. Cut the core to the correct length and grind the end surfaces to level them. The core length should be between 70-75 mm during the experiments.
2. After grinding and cutting, take measurements with a caliper and note down the core's length and diameter. Do also measure the core's weight on a scale. Double-check that the end surfaces of the sample are parallel by measuring the length at different positions of the core's end face.

4.4.2 Preparation of triaxial cell and tubings

1. Make sure the workstation and test equipment are clean and in good shape.
2. For testing without pore pressure:
   Blow through flooding tubings with pressurized air to remove any water/residue from former tests. When the tubings are blown dry, close the inlet and outlet flow valves to isolate the core. This will prevent fluid from leaving the core and tubings during the heating and testing phase, thereby less drying out of the core.
3. For testing with pore pressure:
   Flood inlet and outlet tubings with distilled water and close valves to keep the tubings filled with water until the test starts.

4.4.3 Installation of the core into the triaxial cell

Figure 8: Picture of a core with rubber rings, filter paper, and distributor plates to the left, picture of a core with rubber rings in the middle, and picture of a core installed with extensometer, spiral assembly, and shrinking sleeve to the right.

1. Cut two filter papers with a diameter of 35 mm. This paper should be placed on the side of the distributor plates, not touching the core.
2. Cut the shrinking sleeve to approximately 125 mm and smooth the edges. The sleeve should be long enough to cover at least 10 mm of metal on the base pedestal to 10 mm on the spiral assembly on top of the core.
3. Apply a thin layer of vacuum grease to the areas on the base pedestal and the spiral assembly that the shrinking sleeve will cover.
4. Place a rubber ring slightly onto the base pedestal, then place a cut filter paper into the rubber ring, followed by a distributor plate, Figure 8.
5. Place the core on top of the distributor plate and ensure the rubber ring covers the edge of the core and base pedestal.
6. Install a rubber ring on top of the core. Then place a distributor plate and a filter paper on top of the core.
7. Place the prepared shrinking sleeve over the core.
8. Place the spiral assembly on top of the core. This is done to ensure that the shrinking sleeve fits and to hold the core in place while melting the shrinking sleeve.
9. Melt the shrinking sleeve from the bottom to about 20 mm from the top of the core. Cover the electronics for the extensometer while melting the shrinking sleeve.
10. Remove the spiral assembly and install the extensometer. Place the extensometer and its wires as far down as possible.
11. Reinstall the spiral assembly while making sure the rubber ring covers both the edge of the core and the spiral assembly. Tighten the swagelock fitting on the spiral assembly with the outlet flow tubing coming into the cell.
12. Melt the remaining part of the shrinking sleeve while applying some load on the spiral assembly. When melted, the sleeve should make a tight seal onto the base pedestal, spiral assembly, and core, Figure 8.
13. Move the extensometer to the middle of the core and start LabVIEW. Check the signal from the extensometer in LabVIEW. Ensure that it is within its measuring range and can be compressed and extended without going out of its measuring range.

4.4.4 Assembly of the triaxial cell

Figure 9: Picture of partly assembled and assembled triaxial cell to the left and in the middle. Electric torque wrench from ITH technologies to the right.

1. Close the drainage valve going from the triaxial cell to the waste tank.
2. Install the confining chamber wall over the core and let it rest on the base, Figure 9.
3. Fill the confining chamber with confining oil to about 10 mm from the top. Remove any spilled oil from the outside of the confining chamber wall.
4. Place the heating jacket over the chamber wall. It should be fastened properly approximately on the center of the wall.
5. Install the triaxial cell top onto the confining chamber. Make sure to open a valve on the top connected to the confining chamber to allow excess oil to be removed. Apply some pressure to the top to move it properly in place. When the top is in place, it should be possible to rotate it.
6. Align the holes on the top with the threaded holes in the base. Install the six bolts and hand-tighten them. When all bolts are hand tightened, apply 250 Nm torque to the bolts while going in a cross pattern, Figure 9.
7. Install the LVDT (linear variable differential transformer) onto the axial piston of the triaxial cell. Ensure that the measuring pin moves freely and that the wire to the LVDT does not have contact with the cell if high temperatures are used.
8. Check signals from the LVDT in LabVIEW. Check that it reacts when moving the measuring pin up and down.

4.4.5 Preparations for the triaxial test

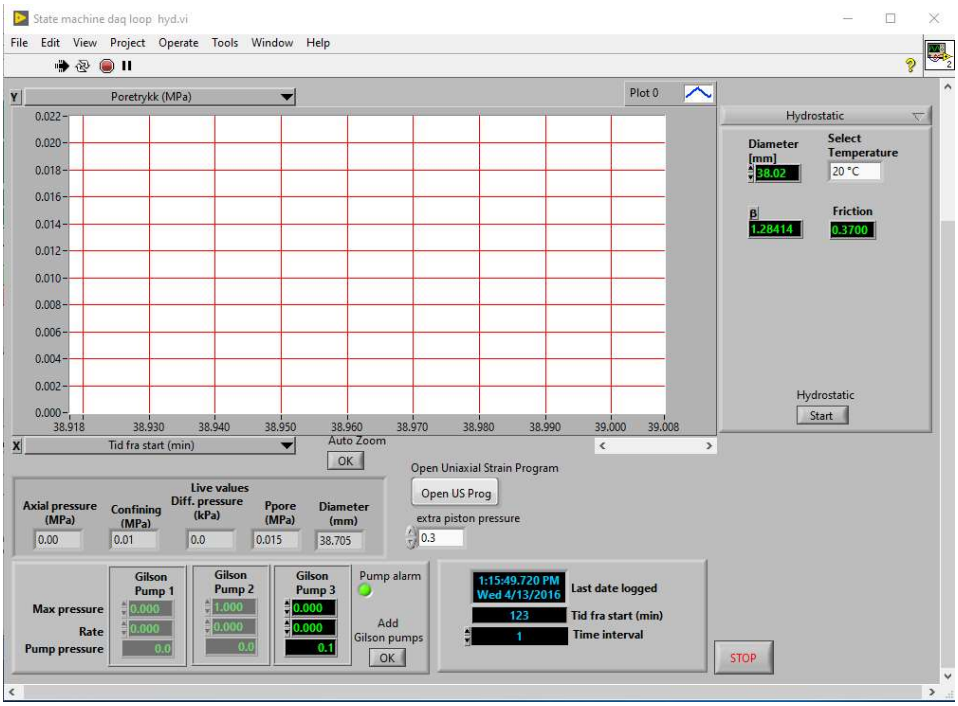

Figure 10: LabVIEW interface

1. Start a new test in LabVIEW, Figure 10, and reset the pressure transducers on the pumps. Set the Y-axis to confining pressure and the X-axis to time.
2. Flush oil into the confining chamber until only oil comes out of the confining outlet valve to ensure no air is left inside the chamber. An appropriate flooding rate for this task is 3 ml/min. Close the confining valve outlet when only oil is being drained.
3. Increase the confining pressure to 0.5 MPa. An appropriate flooding rate for this task is 3 ml/min. When pressure is reached, set the pump in a constant pressure mode to keep the pressure constant at 0.5 MPa.
4. Change the Y-axis to piston pressure and the X-axis to axial movement and set the piston pump safety pressure to 1.5 MPa. Ensure the lower piston chamber inlet valve is closed and the lower piston chamber outlet is open. Flush oil into the upper piston chamber and let it drain from the upper piston chamber outlet. Close the upper piston chamber outlet when only oil is being drained. An appropriate flooding rate for this task is 2 ml/min.
5. When the upper piston chamber outlet valve is closed, the piston pressure will increase to the friction pressure before it starts to move. Oil will be drained from the lower piston chamber outlet when the piston moves downwards. The pump should be stopped manually or by safety pressure when the piston lands on the core. A sudden increase in the piston pressure will indicate this. When the piston has landed on top of the core, set the pump into constant pressure mode to keep the axial pressure constant at a calculated pressure value. Because the friction

pressure increases with increasing confining pressure, a software program will automatically adjust the axial pressure during loading.

6. For testing with pore pressure:
   Increase the confining pressure to 1.2 MPa and the pore pressure to 0.7 MPa simultaneously. The pore pressure should be applied on both sides of the core by opening a bypass valve which makes the pressure equal on both sides of the core. The pressure is controlled using a back pressure regulator controlled by gas pressure.
7. Connect a relief valve to the confining chamber outlet valve. This valve keeps the confining pressure constant at the set pressure during heating. Stop the confining pump and increase the temperature to the target temperature. When a temperature close to the target temperature is reached, the confining pump can be started again, and the relief valve is removed.
8. The temperature should be constant for at least 12 hours before starting the triaxial test.

4.4.6 Hydrostatic phase

1. Change the Y-axis to confining pressure and the X-axis to axial movement.
2. Check radial deformation during loading by changing the X-axis to the extensometer.
3. Increase the confining pressure to the pre-determined confining pressure by 1.67 MPa/min. When the determined confining pressure is reached, keep it constant by a constant pressure mode.

4.4.7 Deviatoric phase

1. Set the Y-axis to piston pressure and the X-axis to axial movement.
2. Increase the piston pressure by 12 MPa/min until the core has failed.
3. When the core has failed, set the piston pump in a constant pressure mode at the pressure the piston currently has.

4.4.8 Ramping down, resetting the piston, and disassembling the triaxial test setup

1. Ramp down the piston pressure to the friction pressure in a controlled manner.
2. For testing without pore pressure:
   Ramp down the confining pressure to 0.5 MPa in a controlled manner.
   For testing with pore pressure:
   Ramp down the confining pressure to 1.2 MPa in a controlled manner.
3. Turn off the heater and wait until the cell cools to an appropriate working temperature.
4. Lift the piston by pumping into the lower piston inlet while the upper piston outlet is open. When lifting the piston, the pressure remains constant until the piston is back at the upper position. The pressure increases when it reaches this position, and the axial movement stops. To avoid a high-pressure spike, apply a safety pressure of 2 MPa to the piston pump. An appropriate pumping rate for this task is 2 ml/min.

5. For testing with pore pressure:

   Decrease the pore pressure from 0.7 MPa to 0 MPa simultaneously as the confining pressure is unloaded from 1.2 MPa to 0.5 MPa. This is performed by gradually removing the applied pressure from the back pressure regulator as the confining pressure is unloading.
6. Open the drainage valve from the confining chamber to the oil tank and apply air pressure to the confining chamber through the confining chamber outlet to empty the oil into the oil tank. Remove the air pressure when the confining chamber is empty.
7. Disassemble the LVDT and remove the bolts. Dismantle the top and confining chamber. Loosen the autoclave on the spiral assembly and remove the spiral assembly from the core. Remove the extensometer from the core. Remove the core from the pedestal and extract it by cutting and removing the shrinking sleeve.
8. Take pictures of the core and measure core mass after testing.

5 Results and discussion

In this chapter, the test results will be compared to see whether applying pore pressure affects the performed tests mechanical strength and elastic modulus. Since a triaxial test is divided into two phases, the results will also be presented on a basis from those phases. During the results and discussion, groups will sometimes be referred to when comparing the results. The experiments performed have been divided into 3 groups which are: the orange group (V1-V4) containing tests performed with 17.2 MPa confining pressure at 90°C, the grey group (V5-V8) containing tests performed with 26 MPa confining pressure at 90°C and the yellow group (V9-V12) containing tests performed with 17.2 MPa confining pressure at 120°C.

5.1 Determination of elastic moduli and mechanical strength

5.1.1 Bulk modulus

The Bulk modulus has been determined by plotting a trendline in the interval from 9 MPa to 13 MPa axial stress in an axial stress vs. volumetric strain plot for 11 of the 12 tests performed. Due to a change in shape after 12 MPa axial stress, the trendline for the remaining test (V6) was plotted between 9 and 12 MPa axial stress. The Bulk modulus was then determined as the rate of increase of the trend line. This way of determining a modulus is called a chord modulus. The Bulk modulus has also been determined by taking an average over the whole hydrostatic phase in the volumetric plots. Both ways to determine the Bulk modulus will be presented, but some tests have shapes that will affect the average bulk modulus.

5.1.2 Young's modulus

Young's modulus has been determined as the rate of increase for a trendline plotted in an interval on the axial stress vs. axial strain curve in the deviatoric loading phase. For all tests performed with 17.2 MPa confining pressure, Young's modulus has been determined in the interval from 18-24 MPa axial stress. For the tests performed at 26 MPa confining pressure, Young's modulus has been determined between 27-31 or between 27-32 MPa axial stress. Young's modulus is determined between 27-31 MPa axial stress for V6 and V8 due to a short elastic region. Since the elastic region was more extended for V5 and V7, the Young's modulus for those tests was determined between 27-32 MPa axial stress.

5.1.3 Poisson's ratio

Poisson's ratio is determined by Equation 2.5, specified in section 3.4.3, and is determined in the same interval that Young's modulus has been determined for all tests.

5.1.4 Mechanical strength

The mechanical yield strength of the samples has been measured by applying a 0.2% offset and determined as the value where the offset crosses the graph for axial strain in the deviatoric phase. The base for the 0.2% offset has been the linear trendline used in Young's modulus calculations.

5.2 Hydrostatic phase

The axial and radial strains were measured during the hydrostatic phase, and the volumetric strain was calculated from the axial and radial strains. Furthermore, the Bulk modulus was defined as described in 5.1.1. The confining pressure applied in the hydrostatic phase was 17.2 MPa for tests V1-V4 and V9-V12, and for tests V5-V8, the applied confining pressure was 26 MPa.

The axial strain will be most focused on during the comparison because it is the most accurate strain measurement. This will be discussed in detail in chapter 5.4.

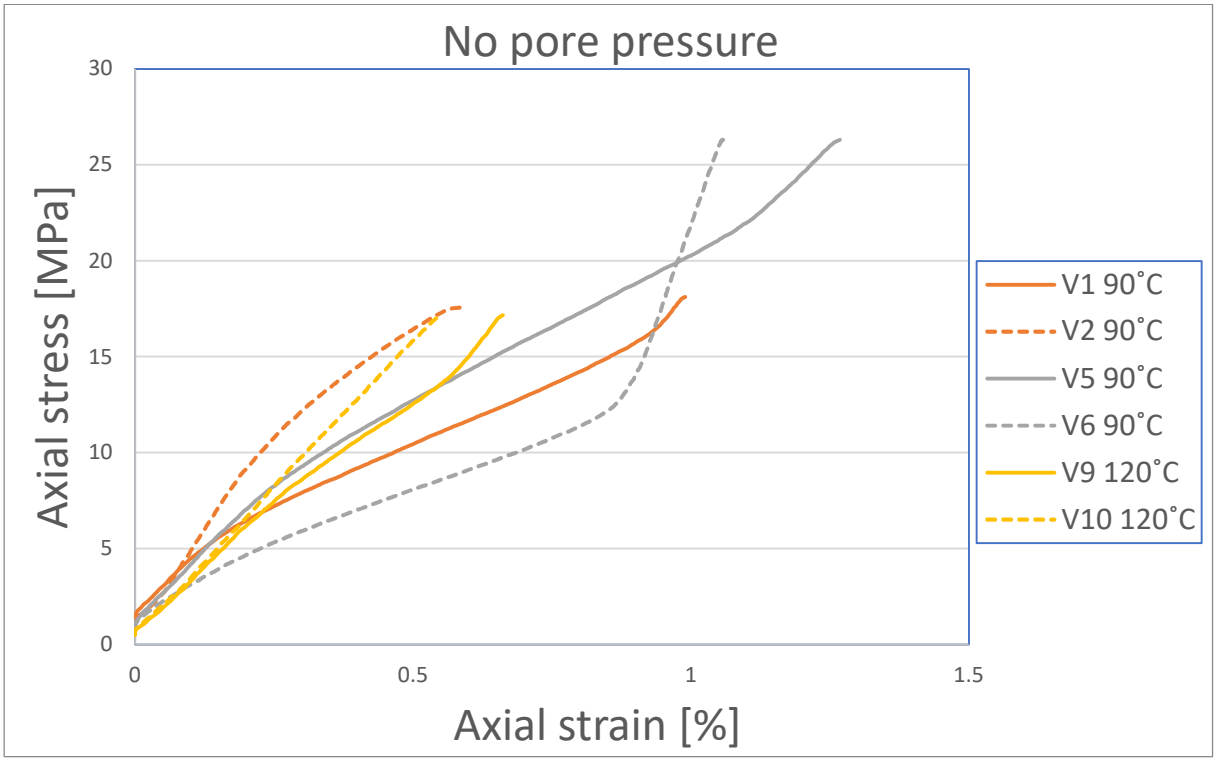

Figure 11: Presentation of axial strain in the hydrostatic phase without pore pressure

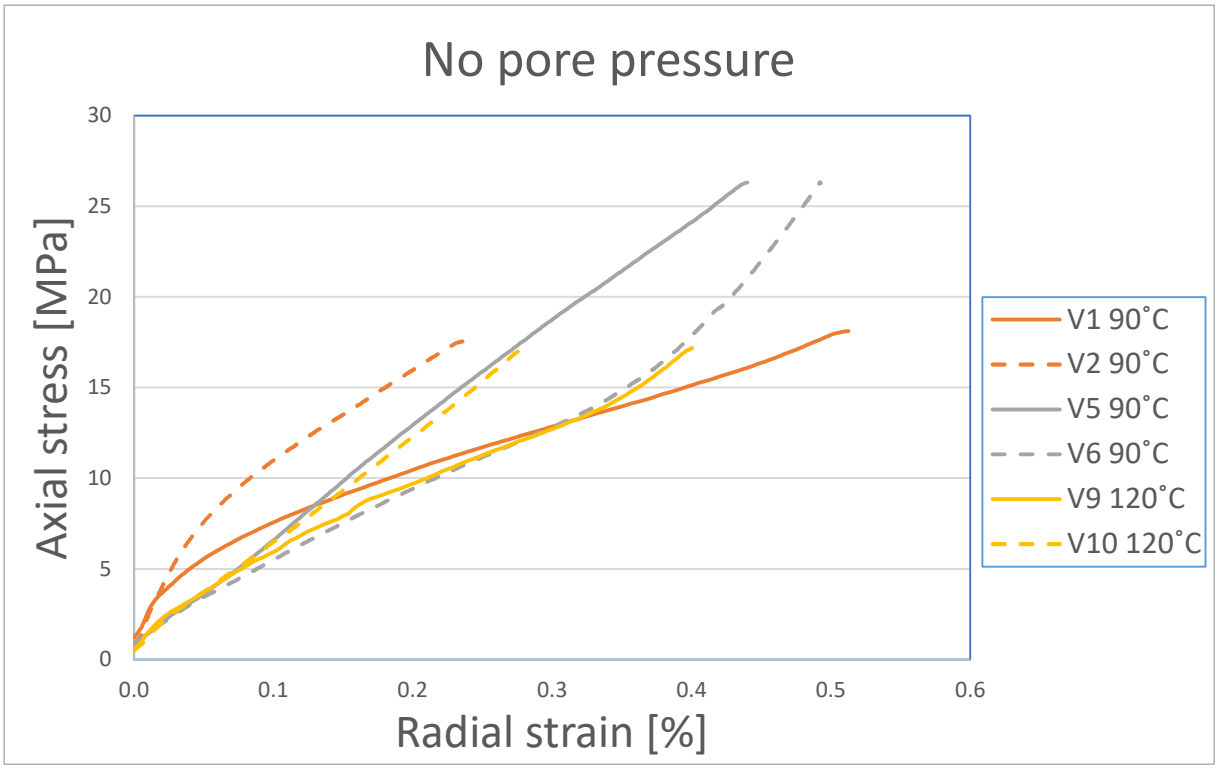

Figure 12: Presentation of radial strain in the hydrostatic phase without pore pressure.

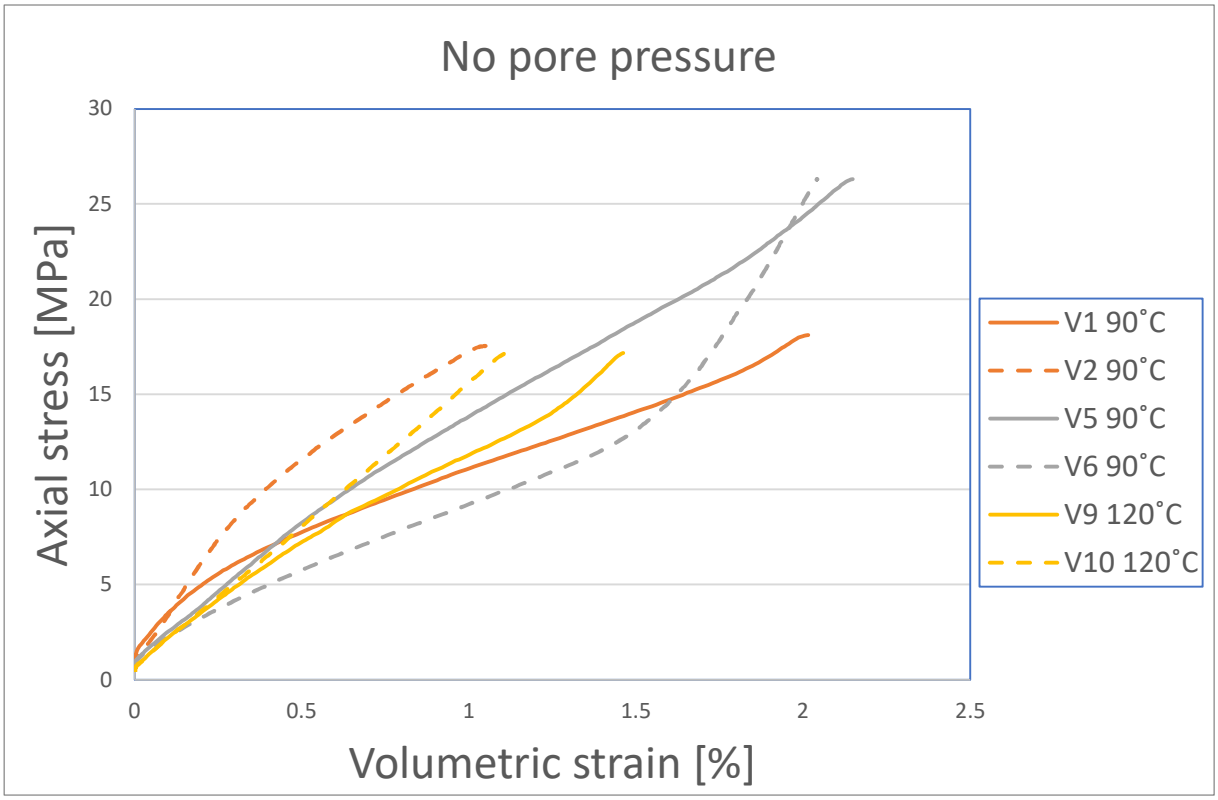

Figure 13: Presentation of volumetric strain in the hydrostatic phase without pore pressure.

The presentation in Figures 11,12, and 13 is of the measurement of strains versus axial stress. The tests performed in the same groups have been assigned the same color to show variation within tests

performed under the same pressure and temperature. The grey- and orange-colored graphs are performed with the same confining pressure and temperature in the hydrostatic phase until 17.2 MPa axial stress is reached.

As shown in Figure 11, the axial stress versus axial strain curves for the triaxial tests performed without pore pressure has several different shapes that seem to be random. These curves make the results less repeatable and significantly impact the Bulk modulus and strains. For example, axial strain at 17.2 MPa at 90°C varies with a factor close to 2, ranging from 0.55% to 1% axial strain.

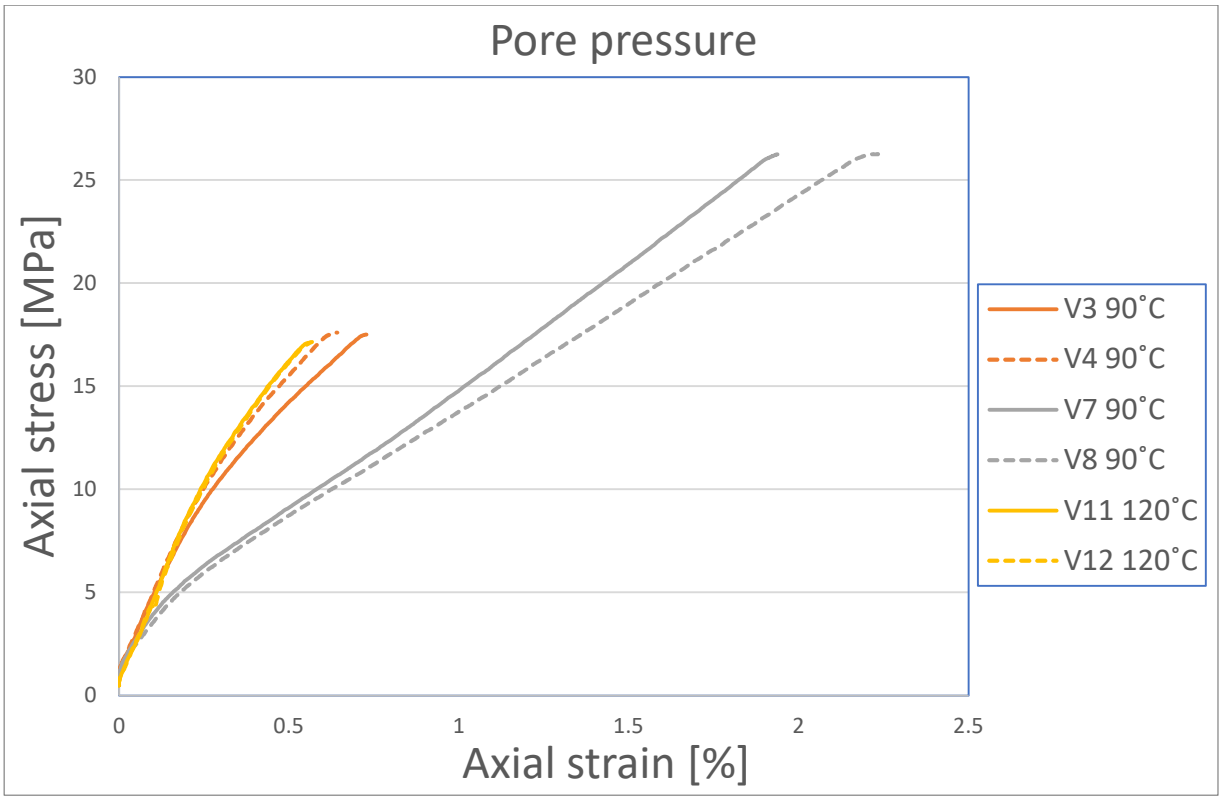

Figure 14: Presentation of axial strain in the hydrostatic phase with pore pressure

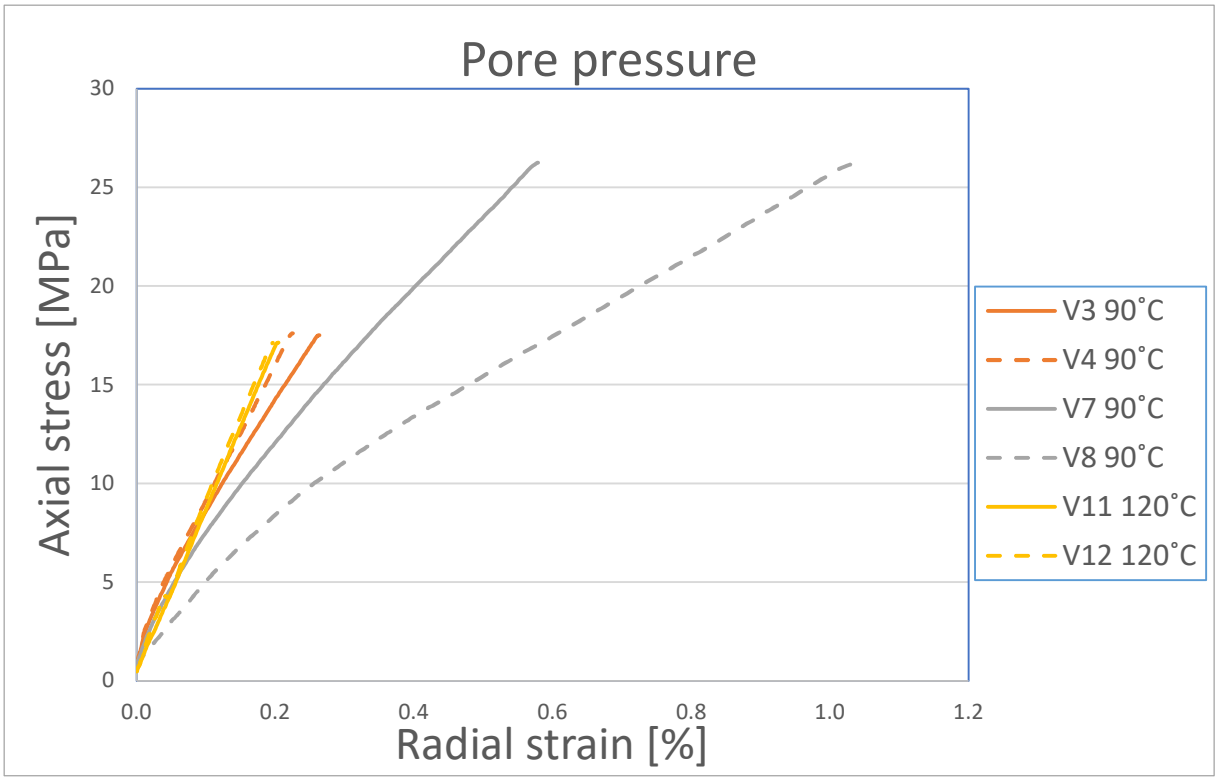

Figure 15: Presentation of radial strain in the hydrostatic phase with pore pressure.

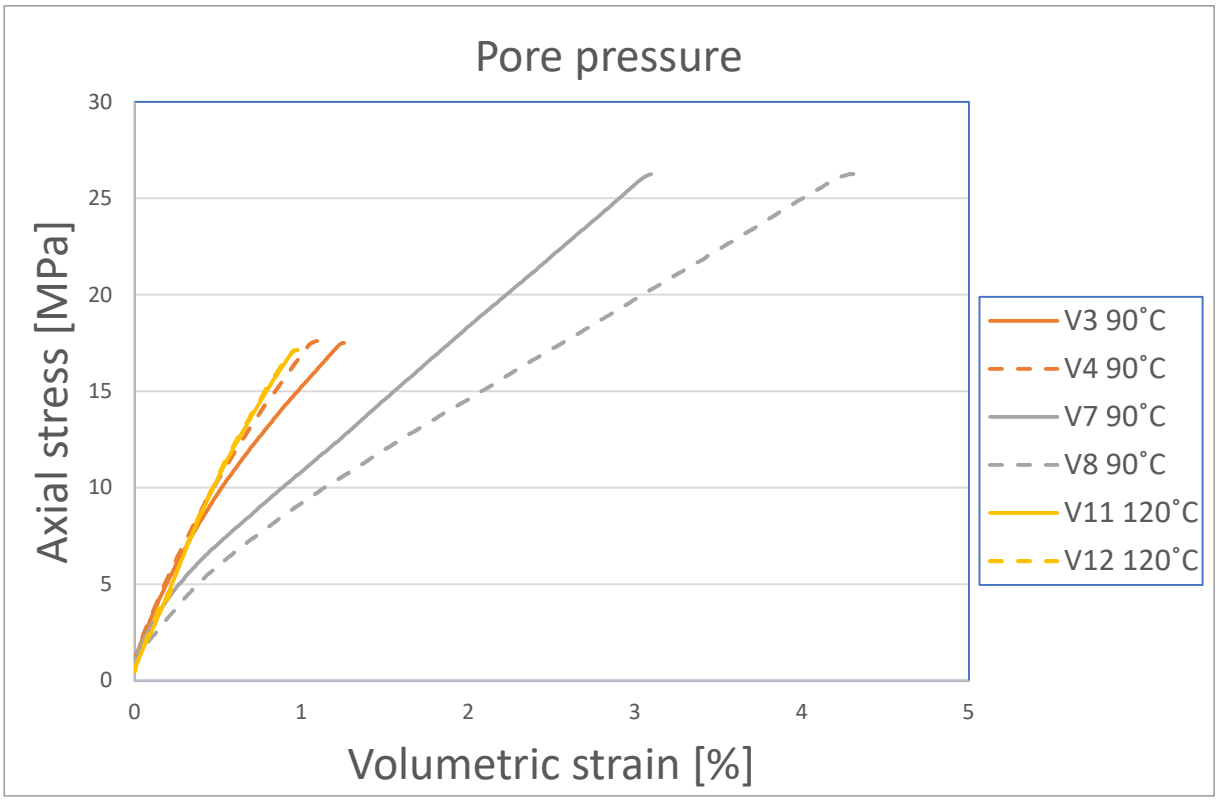

Figure 16: Presentation of volumetric strain in the hydrostatic phase with pore pressure.

Figures 14, 15, and 16 present the results of the triaxial tests performed with applied pore pressure. The test procedure is equal to the ones performed in Figures 11, 12, and 13, except that pore pressure is applied. Figures 14, 15, and 16 show more consistent results, especially considering the linear and repeatable stress versus strain curves. For example, in Figure 14, at 17.2 MPa axial stress, the most significant difference in axial strain for tests performed within the same group was 0.13%. On the other hand, the experiments performed in the orange and the grey groups should have similar results when the axial stress reached 17.2 MPa. But the difference between the average axial strain between the orange and grey graphs with pore pressure applied at 17.2 MPa and 90°C is 0.61% meaning that the grey graphs had almost twice the amount of axial strain as the orange graphs. Due to this significant difference withing tests performed with the same temperature and confining pressure, it seems like a change in the core preparation process has changed the samples properties.

During the project, some minor changes were made to the mixing and curing procedures. In short, when creating sample V6 and forward, the grease used inside the curing molds was changed. When creating sample V7 and forward, the slurry was stirred slightly after conditioning with a spatula. Lastly, from sample V8, no water was added on top of the slurry in the curing mold. These changes are small, but they might very well affect the outcome of the tests performed. Due to the results shown in Figure 14 regarding the orange graphs(V3-V4) and the grey graphs (V7-V8), it seems that the changes have affected the mechanical properties of the cores significantly. Due to the changes in the preparation procedure, the Bulk modulus of the tests in the orange and grey groups will be treated as separate groups when comparing repeatability. When comparing the magnitude of the Bulk modulus, the base for the comparison will be before and after the new preparation procedure. This is because it would be misleading to treat the Bulk modulus determined from the grey and orange groups as the same due to the changes in the preparation procedure. Even though the Bulk modulus for the grey and orange groups have been determined in the same way at the same pressure and temperature, the change in the preparation procedure makes the results quite different.

Table 1: Chord Bulk modulus comparison

Temperature [˚C]	Confining pressure [MPa]	Bulk modulus without pore pressure [GPa]	Bulk modulus with pore pressure [GPa]
90.0	26.0	Sample V5 = 1.11	Sample V7 = 0.73
90.0	26.0	Sample V6 = 0.70	Sample V8 = 0.55
90.0	17.2	Sample V1 = 0.62	Sample V3 = 1.18
90.0	17.2	Sample V2 = 1.42	Sample V4 = 1.45
120.0	17.2	Sample V9 = 0.85	Sample V11 = 1.69
120.0	17.2	Sample V10 = 1.49	Sample V12 = 1.70

Table 2: Average Bulk modulus comparison

Temperature [˚C]	Confining pressure [MPa]	Bulk modulus without Pore pressure [GPa]	Bulk modulus with pore pressure [GPa]
90.0	26.0	Sample V5 = 1.13	Sample V7 = 0.78
90.0	26.0	Sample V6 = 1.08	Sample V8 = 0.57
90.0	17.2	Sample V1 = 0.75	Sample V3 = 1.30
90.0	17.2	Sample V2 = 1.59	Sample V4 = 1.55
120.0	17.2	Sample V9 = 1.05	Sample V11 = 1.78
120.0	17.2	Sample V10 = 1.50	Sample V12 = 1.79

Table 1 and 2 clearly shows improved repeatability for the tests performed with pore pressure applied compared to those without within the groups. The results from Table 1 will be compared to each other in this comparison. The tests performed in the same groups with pore pressure have an average difference in Bulk modulus of 0.153 GPa. 0.153 GPa is a small average difference compared to the tests performed without pore pressure, which had an average difference of 0.617 GPa. There is also less variation in the average difference between Bulk modulus for all tests in the same group performed with pore pressure compared to those without pore pressure. According to these results, applying pore pressure impacts the Bulk modulus and makes it significantly more repeatable.

Another aspect of the Bulk modulus is the small variation of Bulk modulus for the tests performed at 120°C with pore pressure applied, Table 1. The difference between the tests performed with pore pressure applied at 120°C (V11 and 12) was only 0.01 GPa. On the contrary, the tests performed without pore pressure applied at 120°C (V9 and V10) did have Bulk modulus with a difference of 0.64 GPa. The repetitive Bulk modulus of the tests performed at 120°C with pore pressure can have several reasons. It can be that the higher temperatures make the sample stronger, leading to better repeatability when pore pressure is applied, or it can be a coincidence. Lastly, to make a certain conclusion as to whether the increased temperature improves the repeatability of the tests, more tests must be performed at elevated temperatures.

Table 3: Chord Bulk modulus magnitude comparison

Chord Bulk modulus	90℃ old preparation procedure [GPa]				Average [GPa]
With pore pressure	Sample V3 = 1.18	Sample V4 = 1.45			1.32
Without pore pressure	Sample V1 = 0.62	Sample V2 = 1.42	Sample V5 = 1.11	Sample V6 = 0.7	0.96
	90℃ new preparation procedure [GPa]				
With pore pressure	Sample V7 = 0.73	Sample V8 = 0.55			0.64
	120℃ new preparation procedure [GPa]				
With pore pressure	Sample V11 = 1.69	Sample V12 = 1.70			1.7
Without pore pressure	Sample V9 = 0.85	Sample V10 = 1.49			1.17

In Table 3, there is a comparison to show if the Bulk modulus increases or decreases when pore pressure is applied. Since there was a change in the preparation procedure that affected the properties, the change must be taken into the comparison. The change happened between V6-V8, but the change at V8 was to stop adding water on top of the slurry in the curing molds before placing them into the autoclave cell. This change did most likely not have any effect since there is coming water on top of the samples through the hole in the top lid of the curing mold. Due to this, all samples after V6 were made with the updated mixing procedure.

From Table 3 one can see that the samples made with the old preparation process at 90°C had an average Bulk modulus of 1.32 GPa with pore pressure applied, which is higher compared to the samples tested without pore pressure applied, which had an average Bulk modulus of 0.96 GPa. The same trend with increased Bulk modulus is shown for the tests with the new preparation procedure at 120°C, where the samples without pore pressure had 1.17 GPa Bulk modulus, and the samples with pore pressure had 1.7 GPa Bulk modulus. For samples V7-V8, there are no tests performed with the new preparation procedure without pore pressure at 90 °C to compare these tests with. Because of this, it is not possible to make a comparison for the tests performed at 90°C with the new testing procedure. But it is worth noting that the tests with the new testing procedure at 90°C had an average Bulk modulus of 0.64 GPa, the lowest average measured.

To make a certain conclusion about the magnitude of the bulk modulus, the tests performed with the old preparation procedure should be redone with the new preparation procedure. But for the comparisons performed for pore pressure vs. no pore, it seems like applying pore pressure increases the Bulk modulus. It also looks like elevated temperatures increase the Bulk modulus. The Bulk modulus values

for the tests performed at 120°C are the two highest Bulk modulus values measured. Comparing the bulk modulus values with pore pressure applied from the samples created with the new preparation procedure at 120°C with those created with the new preparation procedure at 90°C. The tests at 120°C had an average of 1.7 GPa Bulk modulus, just above 2.5 times the magnitude of the Bulk modulus at 90°C which had an average of 0.64 GPa. This strongly indicates that the Bulk modulus increases at elevated temperatures.

Table 4: Total strain under hydrostatic loading comparison

Sample number	Temperature [˚C]	Confining pressure [MPa]	Axial strain [%]	radial strain [%]	Pore pressure
V5	90.0	26.0	1.27	0.44	no
V6	90.0	26.0	1.06	0.49	no
V7	90.0	26.0	1.94	0.58	yes
V8	90.0	26.0	2.23	1.05	yes
V1	90.0	17.2	0.99	0.51	no
V2	90.0	17.2	0.59	0.24	no
V3	90.0	17.2	0.73	0.26	yes
V4	90.0	17.2	0.64	0.23	yes
V9	120.0	17.2	0.66	0.40	no
V10	120.0	17.2	0.55	0.28	no
V11	120.0	17.2	0.57	0.20	yes
V12	120.0	17.2	0.56	0.20	yes

Table 4 presents the axial and radial strain for all the tests performed. The comparison below will focus on the axial strain as it is the most accurate of the strain measurements due to the description in section 5.4. The tests with pore pressure applied had an average of 0.13% difference in axial strain for the tests performed in the same groups. These results show that applying pore pressure provides better repeatability for the axial strain, as the average difference for the tests performed in the groups without pore pressure was 0.24%. Since the Bulk modulus is calculated from the slope of the stress-strain curves, the results from Bulk modulus and strains should be expected to indicate the same trends.

Furthermore, the strain values also show that the best repeatability of the tests performed is for the tests at 120°C with pore pressure applied. This will likely be because of the same reasons discussed for the Bulk modulus at elevated temperatures.

Lastly, the tests performed at 120°C with pore pressure had an average Bulk modulus of 1.70 GPa and an average axial strain of 0.57%. The Bulk modulus is the highest average, and the axial strain is the lowest average that is measured in tests performed with the same temperature and confining pressure. This indicates that the elevated temperature makes the samples stronger. But more tests should be done to make a reliable conclusion due to the small sample size.

Table 5: Chord Bulk modulus calculated by only axial strains comparison

Temperature [˚C]	Confining pressure [MPa]	Bulk modulus without pore pressure [GPa]	Bulk modulus with pore pressure [GPa]
90.0	26.0	Sample V5 = 0.57	Sample V7 = 0.37
90.0	26.0	Sample V6 = 0.39	Sample V8 = 0.33
90.0	17.2	Sample V1 = 0.41	Sample V3 = 0.68
90.0	17.2	Sample V2 = 0.96	Sample V4 = 0.85
120.0	17.2	Sample V9 = 0.65	Sample V11 = 0.94
120.0	17.2	Sample V10 = 1.00	Sample V12 = 0.94

Table 6: Average Bulk modulus calculated by only axial strains comparison

Temperature [˚C]	Confining pressure [MPa]	Bulk modulus without pore_pressure [GPa]	Bulk modulus with pore pressure [GPa]
90.0	26.0	Sample V5 = 0.61	Sample V7 = 0.41
90.0	26.0	Sample V6 = 0.68	Sample V8 = 0.36
90.0	17.2	Sample V1 = 0.50	Sample V3 =0.75
90.0	17.2	Sample V2 = 0.99	Sample V4 =0.90
120.0	17.2	Sample V9 = 0.79	Sample V11 = 1.03
120.0	17.2	Sample V10 = 1.02	Sample V12 = 1.03

Tables 5 and 6 present the Bulk modulus determined by axial strains only. The Bulk modulus is determined as specified in section 5.1.1, but these Bulk modulus values are determined from volumetric plots where the volumetric strain is calculated as $3 * axial\ strain$ instead of $axial\ strain + 2 * radiel\ strain$. These tables were made to check if the radial strain measurements affected the Bulk modulus.

When comparing, the focus will be on Table 5. The tests performed within the same group without pore pressure have an average difference in Bulk modulus of 0.36 GPa. On the other hand, the tests performed with pore pressure only had an average difference of 0.07 GPa. When comparing these results, applying pore pressure seems to improve the Bulk modulus's repeatability. There was also a high degree of repeatability for the tests performed with pore pressure at 120 ℃ with 0 GPa difference in the Bulk modulus. These results tell the same story as those presented in Tables 1 and 2.

5.3 Deviatoric phase

After the defined confining pressure is reached, the deviatoric phase is started. During this phase, the axial stress is raised at a constant rate until the sample fails. In my experiments, no sample failed by shear failure. After loading above the yield stress, all samples showed ductile behavior, Figures 17 and 18. Further loading just compressed the sample further in the ductile region. Strain hardening was observed in all tests. Due to this, the tests were usually stopped when the extensometer went out of range.

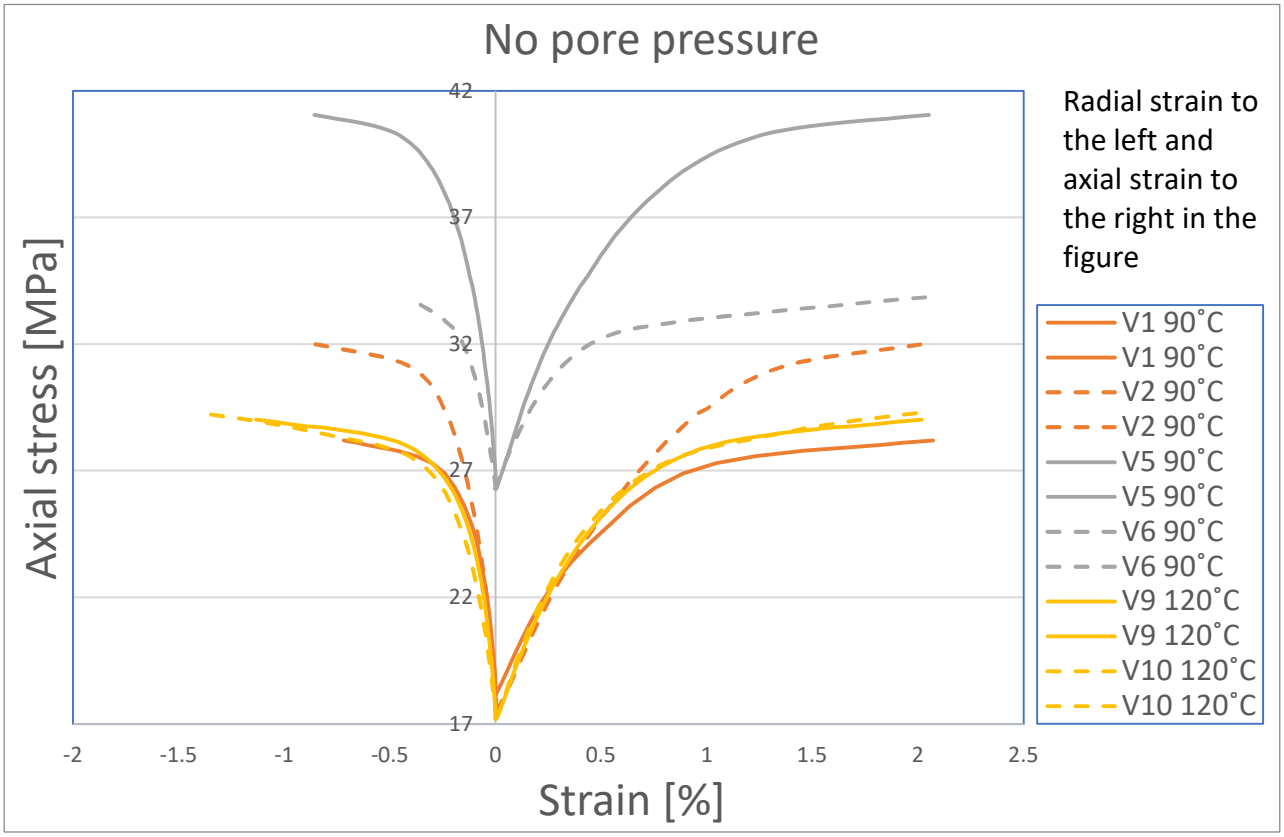

Figure 17: Deviatoric phase of tests performed without pore pressure

Figure 17 and Table 7 show the results from the deviatoric loading phase for all tests without applying pore pressure. The test performed within the same group has the same color to make the difference between tests performed with the same temperature and confining pressure visible. This diagram shows a significant difference of 8.4 MPa mechanical strength in the tests performed with 26 MPa confining pressure at 90˚C. There was also a 2.5 MPa mechanical strength difference between the tests performed at 17.2 MPa at 90˚C. Lastly, the loading curves for the tests performed at 17.2 MPa confining pressure at 120˚C were almost equal. The reason for the last two tests being equal might be a coincidence, an effect of the temperature, or due to the changes made to the sample preparation procedures. The differences are quite significant for the other tests, and for a barrier material, we might wish to have a material that repeatedly provides the same test results.

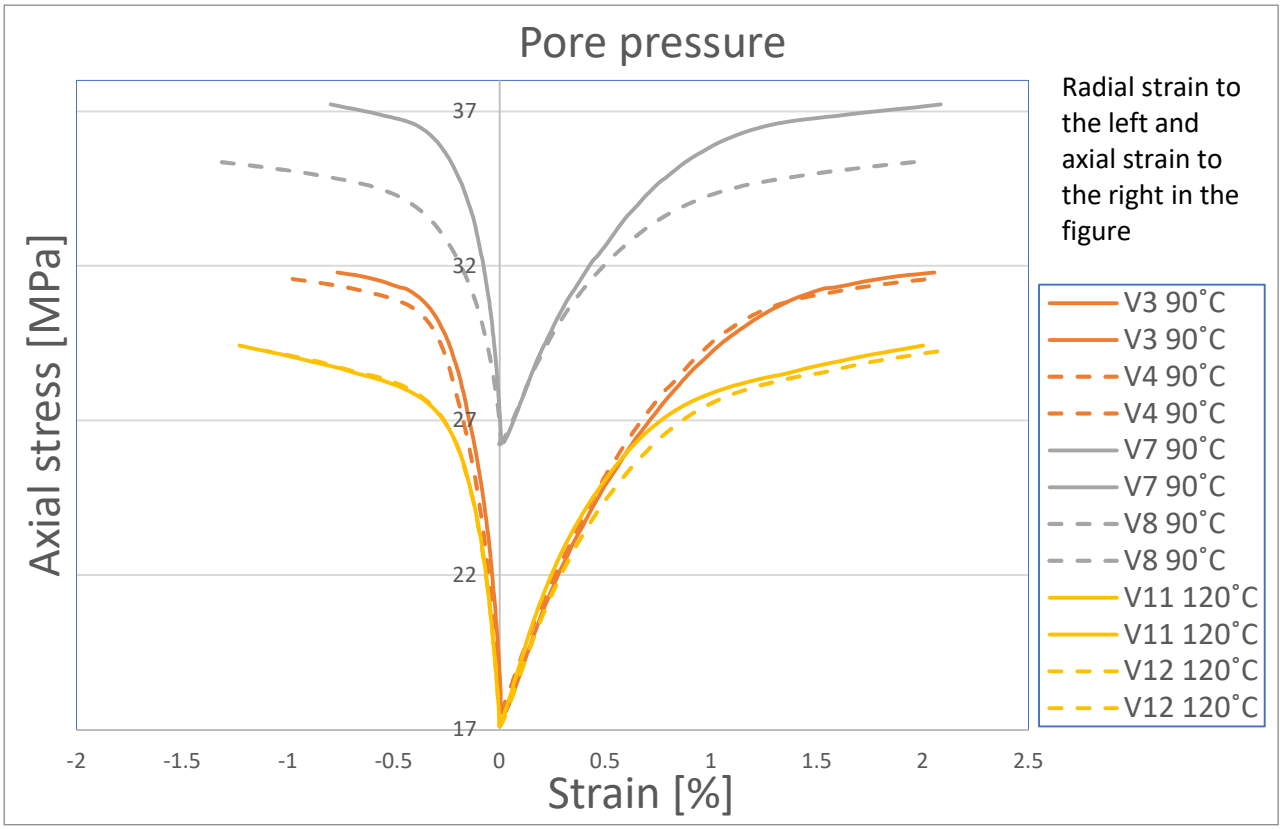

Figure 18: Deviatoric phase of tests performed with pore pressure

Figure 18 and Table 7 present all the deviatoric tests performed with pore pressure applied. The tests are performed under the same temperatures and confining pressure as those in Figure 17, except for the applied pore pressure. All tests performed at 17.2 MPa with pore pressure show good repeatability with similar loading curves where the difference in mechanical strength is 0.55 MPa at 90°C and 0 MPa at 120°C. But there is still a significant difference in the mechanical strength between the tests performed at 26 MPa confining pressure of 1.65 MPa. The results from the tests with pore pressure compared to those without strongly indicate that applying pore pressure makes the tests more repeatable and reliable. The differences between tests performed with the same temperature and confining pressure are significantly less for the test performed with pore pressure applied.

Table 7: Comparison of mechanical strength with 0.2% offset

Temperature [˚C]	Confining pressure [MPa]	Mechanical strength at 0.2% offset without pore pressure applied [MPa]	Mechanical strength at 0.2% offset with pore pressure applied [MPa]
90.0	26.0	Sample V5 = 40.05	Sample V7 = 35.10
90.0	26.0	Sample V6 = 32.45	Sample V8 = 33.45
90.0	17.2	Sample V1 = 26.10	Sample V3 = 28.70
90.0	17.2	Sample V2 = 28.60	Sample V4 = 29.25
120.0	17.2	Sample V9 = 27.15	Sample V11 = 26.80
120.0	17.2	Sample V10 = 27.00	Sample V12 = 26.80

Table 7 acts as a comparison of Figure 17 and Figure 18 concerning mechanical strength. It was chosen to make a 0.2% offset of the tangent used to calculate Young's modulus to determine the mechanical strength of the samples. This choice was made to treat every test the same way, and it gives an estimate of the mechanical strength of the samples without having any other factors affecting the value. The comparison in Table 7 shows the same results as Figures 17 and 18, this being that it seems like the pore pressure can produce more repeatable tests. By repeatable, it means that the mechanical strengths of the tests performed with pore pressure with the same temperature and pressure are similar. The tests performed without pore pressure had a higher gap between the values and looks to be less repeatable. As for the average mechanical strength, there does not seem to be a significant difference between tests with or without pore pressure applied. If there is a difference between the average mechanical strength, it would be necessary to perform more tests to make any conclusion.

Table 8: Comparison of Young's modulus

Temperature [˚C]	Confining pressure [MPa]	Young's modulus without pore pressure [GPa]	Young's modulus with pore pressure [GPa]
90.0	26.0	Sample V5 = 2.33	Sample V7 = 1.40
90.0	26.0	Sample V6 = 1.52	Sample V8 = 1.30
90.0	17.2	Sample V1 = 1.53	Sample V3 = 1.65
90.0	17.2	Sample V2 = 1.65	Sample V4 = 1.59
120.0	17.2	Sample V9 = 1.68	Sample V11 = 1.76
120.0	17.2	Sample V10 = 1.73	Sample V12 = 1.49

Furthermore, in Table 8, there is a comparison of Young's modulus for all tests with and without pore pressure. The average difference in Young's modulus for tests performed with the same temperature and pressure without pore pressure is 0.33 GPa. When comparing the tests without pore pressure with those with pore pressure applied, where the difference was 0.14 GPa, it does look like applying pore pressure makes Young's modulus more repeatable. But it isn't easy to conclude because of the spread of the results, where V9-V12 showed less variation for the tests performed without pore than the tests performed with. Due to the results, more experiments need to be done to make a reliable conclusion as to whether applying pore pressure makes Young's modulus more repeatable.

Table 9: Magnitude comparison of Young's modulus

Young's modulus	90℃ old preparation procedure with 17.2 MPa confining [GPa]		Average [GPa]
With pore pressure	Sample V3 = 1.65	Sample V4 = 1.59	1.62
Without pore pressure	Sample V1 = 1.53	Sample V2 = 1.65	1.59
	90℃ new preparation procedure with 26 MPa confining [GPa]		
With pore pressure	Sample V7 = 1.40	Sample V8 = 1.30	1.35
	120℃ new preparation procedure with 17.2 MPa confining [GPa]		
With pore pressure	Sample V11 = 1.76	Sample V12 = 1.49	1.63
Without pore pressure	Sample V9 = 1.68	Sample V10 = 1.73	1.71

Table 9 shows a comparison of the average Young's modulus. Since there was a change in the core preparation procedure, the values from samples V5 and V6 will not be a part of the comparison because they were performed at 26 MPa confining pressure with the old preparation procedure.

For the tests performed with the old procedure at 17.2 MPa confining pressure at 90℃, the average Young's modulus for tests with pore pressure was 1.62 GPa. 1.62 GPa is close to 1.59 GPa, which is the average Young's modulus for the test performed without pore pressure applied. For the tests performed with the new testing procedure at 17.2 MPa confining pressure and 120℃, there is a minor difference between 1.63 GPa, which is the average Young's modulus with pore pressure applied, compared to 1.71 GPa, which is the average Young's modulus without pore pressure applied. These results indicate that the magnitude of the Young's modulus is not affected by pore pressure. Due to the change in the preparation procedure, there are no tests that the tests performed with the new testing procedure at 26 MPa confining pressure and 90℃ can be compared to. The average of those tests was 1.35 GPa, the lowest Bulk modulus of the tests performed.

Table 10: Poisson's modulus comparison

Temperature [˚C]	Confining pressure [MPa]	Poisson's ratio without pore pressure	Poisson's ratio with pore pressure
90.0	26.0	Sample V5 = 0.29	Sample V7 = 0.22
90.0	26.0	Sample V6 = 0.36	Sample V8 = 0.40
90.0	17.2	Sample V1 = 0.23	Sample V3 = 0.20
90.0	17.2	Sample V2 = 0.21	Sample V4 = 0.24
120.0	17.2	Sample V9 = 0.29	Sample V11 = 0.30
120.0	17.2	Sample V10 = 0.40	Sample V12 = 0.27

Table 10 compares the Poisson's ratio for tests performed with and without pore pressure. From the comparison, the results seem to be random, between 0.2-0.4, and there does not seem to be a link if pore pressure is applied or not. On the other hand, the numbers can be compared versus where the deformation has taken place on the sample. Some of the samples have the most deformation at the top of the samples, and some have a more barrel-looking shape with deformation in the middle, Figure 20. When comparing the results to the shape, it looks like the samples with the highest Poisson's ratio are barrel formed. This should be expected since the extensometer is placed in the middle of the samples and will provide a higher radial strain measurement when the radial deformation occurs in the middle.

5.4 Experimental weaknesses

- While creating the samples, there were 3 changes in the preparation procedures. In Figure 14, the gray (V7-V8) and orange (V3-V4) graphs are performed with similar test procedures and should have shown similar behavior until 17.2 MPa confining pressure was achieved. Since the orange and grey graphs show quite different results, it seems like the sample properties have changed somewhere between samples V4 and V7. The change in properties is likely connected to the changes that were made to the core preparation process:
    - The first change took place when creating sample V6. Due to some issues with removing samples from the curing molds, the silicon grease used inside the curing mold was changed. The replacement was a multi-purpose lubricant from Industrial oils unlimited with the name Superfilm HI-TEMP extreme pressure grease.

      During the removal of the 5 first samples from the curing molds after curing, there were occasions when the samples were stuck inside the curing mold. When a sample was stuck, it was extracted by pushing and moving it inside the mold until it loosened. When a stuck sample was removed, it often had some damage, and the molds had geopolymers bonded on the inside.

      Of the tests performed in this project, only test number 5 was affected by damage from being stuck in the mold. Sample number V5 was still used as the damage was not too extensive. As shown in Figure 19, an additional small shrinking sleeve was placed over the damage to mitigate the risk of puncturing the shrinking sleeve that separates the pore and confining pressure.

      It is unclear why the silicon grease didn't perform as wanted, but one theory is that the silicon had been oxidized due to a small hole in the silicon grease tube. The problem with geopolymers bonding to the curing molds was absent after sample V5 was extracted. It is also worth noting that the condition of the outer surface was improved when changing grease as the surface became much smoother.

Figure 19: Picture of sample V5 before and after testing

- The second change was that the slurry was slightly stirred with a spatula after the conditioning was finished before pouring the slurry into the curing molds. The reason for this change was because it was experienced that the slurry was thicker on the bottom. This means that the last sample poured would have a thicker consistency than the first sample poured. There were no issues with the consistency of the slurry after the stirring was added to the preparation procedure. The stirring was performed from sample V7.
- The third change was performed from sample V8. This change was to stop adding water on top of the slurry in the curing mold before placing the top lid. This change did not likely have any effect since the slurry would get water on top of top anyways when the curing molds were placed in the autoclave cell and pressurized.

- The radial strain was measured by an extensometer placed in the middle of the core, Figure 8. This is an uncertainty because the cores must deform the same way for every test to yield the same results for radial strain. During the experiments, the observed core deformation varied and was not perfectly centered every time. In Figure 20, there are pictures of 3 plugs with varying radial strain. This off-center strain does affect the radial strain, Bulk modulus, and Poisson's ratio. If two cores have similar axial strain, but one fails more in the top part and the second one gets a barrel shape, the one with the barrel shape will measure more radial strain, which will affect Poisson's measurements. On the other hand, it will not affect axial strain, yield strength, and Young's modulus measurements.

Figure 20: Pictures of V5, V6, and V7. V5 is placed to the left

- All the cores failed radially from the center and up during the experiments, Figure 20. There were no cores that failed radially in the lower half. It is unknown why this happened, but a theory can be that there was some settling after the slurry was placed in the curing molds that might have affected the density/porosity of the top part of the samples.

6 Conclusion

The aim of this experimental work has been to determine the effects of the presence of pore pressure or its lack on rock mechanical properties of the one-part granite-based geopolymers. The idea is that a sample can have a drying-out effect when tested without pore pressure, where water from the samples moves from the core and into the connected tubings. A drying-out effect would most likely happen at high temperatures when water is boiling but it can also occur at lower temperatures. This work has been done to check if the standard procedure for testing the geopolymers should include the application of pore pressure or if it is unnecessary. As a result of this work, the following conclusions can be drawn and should be considered when developing the standard procedures.

- Applying pore pressure affects rock mechanical behavior of the tested geopolymers during the hydrostatic loading phase. The tests performed with pore pressure had linear and repeatable stress versus strain curves that did not change form during the hydrostatic loading phase. On the contrary, the tests performed without applied pore pressure had loading curves with several different shapes.
- The core preparation procedure was changed from sample number V7. The change affected the core's properties and significantly affected the Bulk modulus and strains. It did most likely also affect the shape of the graphs as well. Due to these changes, some results are presented with respect to whether the tests are done with the new or with the old core preparation procedure instead of comparing the results based on the groups.
- The repeatability of the results for the Bulk modulus and measured strains is improved when pore pressure is applied. The repeatability gets more consistent when the testing temperature is elevated to 120°C.
- The Bulk modulus had higher values for the tests performed with pore pressure applied compared to those without. The test performed with pore pressure at 120°C did have the highest average Bulk modulus measured.
- Increasing the temperature to 120°C and applying pore pressure resulted in the highest average Bulk modulus and least average strain compared to all tests conducted at lower temperatures. This indicates that the elevated temperatures make the samples stronger.
- During the deviatoric phase, the tests performed with applied pore pressure had more repeatable results. Compared to those without pore pressure, the tests with pore pressure had much more similar mechanical strength and looking graphs within each group of tests. This favors performing the tests with pore pressure, but it might be necessary with more experiments to make a more certain conclusion.

- It did seem like applying pore pressure made Young's modulus more repeatable, but it did not seem to affect the magnitude of Young's modulus. More experiments must be performed to make a certain conclusion.
- Applying pore pressure does not affect Poisson's ratio of geopolymers.

7 Recommendations for further work

During the hydrostatic and deviatoric phases, the tests performed at 120℃ with pore pressure showed more repeatable results than those performed at 120℃ without pore pressure. During this experimental work, there were only performed 4 tests at 120℃, which is a small sample size to make a reliable conclusion. Based on the results of the effect on Bulk modulus, axial strains, radial strains, the shape of graphs, and mechanical strength observed at 120℃, I would propose further testing at 120℃ or higher temperatures. Further testing would make it possible to make a more reliable conclusion on the effect of pore pressure at high temperatures. This would be helpful when deciding whether it is necessary to apply pore pressure on tests performed at elevated temperatures.

I would also recommend doing all the tests with the same procedure used from sample V7. In this project, there has been a change in the properties of the samples that have affected the results. Performing all the experiments with the same preparation procedure would allow for comparison without considering different preparation procedures. This would strengthen and improve the conclusions.

References

Awoyera, P. O., Adesina, A., Sivakrishna, A., Gobinath, R., Kumar, K. R., & Srinivas, A. (2020). Alkali activated binders: Challenges and opportunities. *Materials Today: Proceedings*, *27*, 40-43. https://doi.org/https://doi.org/10.1016/j.matpr.2019.08.199

Fjær, E., Holt, R. M., Horsrud, P., Raaen, A. M., & Risnes, R. (2008a). Chapter 1 Elasticity. In E. Fjær, R. M. Holt, P. Horsrud, A. M. Raaen, & R. Risnes (Eds.), *Developments in Petroleum Science* (Vol. 53, pp. 1-54). Elsevier. https://doi.org/https://doi.org/10.1016/S0376-7361(07)53001-3

Fjær, E., Holt, R. M., Horsrud, P., Raaen, A. M., & Risnes, R. (2008b). Chapter 2 Failure mechanics. In E. Fjær, R. M. Holt, P. Horsrud, A. M. Raaen, & R. Risnes (Eds.), *Developments in Petroleum Science* (Vol. 53, pp. 55-102). Elsevier. https://doi.org/https://doi.org/10.1016/S0376-7361(07)53002-5

Fjær, E., Holt, R. M., Horsrud, P., Raaen, A. M., & Risnes, R. (2008c). Chapter 3 Geological aspects of petroleum related rock mechanics. In E. Fjær, R. M. Holt, P. Horsrud, A. M. Raaen, & R. Risnes (Eds.), *Developments in Petroleum Science* (Vol. 53, pp. 103-133). Elsevier. https://doi.org/https://doi.org/10.1016/S0376-7361(07)53003-7

Hamie, H., Hoayek, A., El-Ghoul, B., & Khalifeh, M. (2022). Application of non-parametric statistical methods to predict pumpability of geopolymers for well cementing. *Journal of Petroleum Science and Engineering*, *212*, 110333. https://doi.org/https://doi.org/10.1016/j.petrol.2022.110333

Jafariesfad, N., Khalifeh, M., Skalle, P., & Geiker, M. R. (2017). Nanorubber-modified cement system for oil and gas well cementing application. *Journal of Natural Gas Science and Engineering*, *47*, 91-100. https://doi.org/https://doi.org/10.1016/j.jngse.2017.10.002

Kamali, M., Khalifeh, M., Saasen, A., & Delabroy, L. (2020). *Materials for Well Integrity – Short-Term Mechanical Properties of Cement Systems* SPE Norway Subsurface Conference, https://doi.org/10.2118/200739-MS

Kamali, M., Khalifeh, M., Saasen, A., Godøy, R., & Delabroy, L. (2021). Alternative setting materials for primary cementing and zonal isolation – Laboratory evaluation of rheological and mechanical properties. *Journal of Petroleum Science and Engineering*, *201*, 108455. https://doi.org/https://doi.org/10.1016/j.petrol.2021.108455

Khale, D., & Chaudhary, R. (2007). Mechanism of Geopolymerization and Factors Influencing Its Development: A Review. *Journal of Materials Science*, *42*, 729-746. https://doi.org/10.1007/s10853-006-0401-4

Khalifeh, M. (2016). *Materials for optimized P&A performance: Potential utilization of geopolymers. PhD dissertation at the University of Stavanger, Faculty of Science and Engineering* (Publication Number PhD thesis UIS;292) University of Stavanger]. Stavanger. https://uis.brage.unit.no/uis-xmlui/handle/11250/2396282

Khalifeh, M., Hodne, H., Saasen, A., & Vralstad, T. (2013). *Techniques and Materials for North Sea Plug and Abandonment Operations* Offshore Technology Conference, https://doi.org/10.4043/23915-MS

Khalifeh, M., & Saasen, A. (2020). Introduction to Permanent Plug and Abandonment of Wells. *Ocean Engineering & Oceanography*. https://doi.org/10.1007/978-3-030-39970-2

Khalifeh, M., Saasen, A., Hodne, H., & Motra, H. B. (2019). Laboratory evaluation of rock-based geopolymers for zonal isolation and permanent P&A applications. *Journal of Petroleum Science and Engineering*, *175*, 352-362. https://doi.org/https://doi.org/10.1016/j.petrol.2018.12.065

Khalifeh, M., Saasen, A., Vralstad, T., & Hodne, H. (2014). Potential utilization of class C fly ash-based geopolymer in oil well cementing operations. *Cement and Concrete Composites*, *53*, 10-17. https://doi.org/https://doi.org/10.1016/j.cemconcomp.2014.06.014

Khalifeh, M., Todorovic, J., Vrålstad, T., Saasen, A., & Hodne, H. (2017). Long-term durability of rock-based geopolymers aged at downhole conditions for oil well cementing operations. *Journal of Sustainable Cement-Based Materials*, *6*(4), 217-230. https://doi.org/10.1080/21650373.2016.1196466

Lade, P. V. (2016). *Triaxial Testing of Soils*. John Wiley & Sons, Incorporated. http://ebookcentral.proquest.com/lib/uisbib/detail.action?docID=4451906
Ling, Y., Wang, K., Wang, X., & Li, W. (2021). Prediction of engineering properties of fly ash-based geopolymer using artificial neural networks. *Neural Computing and Applications*, *33*(1), 85-105. https://doi.org/10.1007/s00521-019-04662-3
Liu, G. (2021). *Applied Well Cementing Engineering*. San Diego: Elsevier Science & Technology. https://doi.org/10.1016/C2019-0-03030-0
Liu, X., Nair, S. D., Aughenbaugh, K. L., Juenger, M. C. G., & van Oort, E. (2020). Improving the rheological properties of alkali-activated geopolymers using non-aqueous fluids for well cementing and lost circulation control purposes. *Journal of Petroleum Science and Engineering*, *195*, 107555. https://doi.org/https://doi.org/10.1016/j.petrol.2020.107555
Mitchell, R. F., & Miska, S. Z. (2010). *Fundamentals of Drilling Engineering*. Society of Petroleum Engineers. http://ebookcentral.proquest.com/lib/uisbib/detail.action?docID=3404993
Nermoen, A., Korsnes, R. I., Aursjø, O., Madland, M. V., Kjørslevik, T. A. C., & Østensen, G. (2016). How Stress and Temperature Conditions Affect Rock-Fluid Chemistry and Mechanical Deformation. *Frontiers in Physics*, *4*. https://doi.org/10.3389/fphy.2016.00002
Norge, S. (2021). NORSOK D-010. Well integrity in drilling and well operations *5thed., Standards Norway, Lysaker, Norway.*
Pacheco-Torgal, F., Castro-Gomes, J., & Jalali, S. (2008). Alkali-activated binders: A review: Part 1. Historical background, terminology, reaction mechanisms and hydration products. *Construction and Building Materials*, *22*(7), 1305-1314. https://doi.org/https://doi.org/10.1016/j.conbuildmat.2007.10.015
Panchmatia, P., Olvera, R., Genedy, M., Juenger, M. C. G., & van Oort, E. (2020). Shrinkage behavior of Portland and geopolymer cements at elevated temperature and pressure. *Journal of Petroleum Science and Engineering*, *195*, 107884. https://doi.org/https://doi.org/10.1016/j.petrol.2020.107884
Salehi, S., Khattak, J., Saleh, F. K., & Igbojekwe, S. (2019). Investigation of mix design and properties of geopolymers for application as wellbore cement. *Journal of Petroleum Science and Engineering*, *178*, 133-139. https://doi.org/https://doi.org/10.1016/j.petrol.2019.03.031
Salehi, S., Khattak, M. J., Rizvi, H., Karbalaei, S. F., & Kiran, R. (2017). Sensitivity analysis of fly ash geopolymer cement slurries: Implications for oil and gas wells cementing applications. *Journal of Natural Gas Science and Engineering*, *37*, 116-125. https://doi.org/https://doi.org/10.1016/j.jngse.2016.11.025
van Oort, E., Juenger, M., Liu, X., & McDonald, M. (2019). *Silicate-Activated Geopolymer Alternatives to Portland Cement for Thermal Well Integrity* SPE Thermal Well Integrity and Design Symposium, https://doi.org/10.2118/199787-MS
Vrålstad, T., Saasen, A., Fjær, E., Øia, T., Ytrehus, J. D., & Khalifeh, M. (2019). Plug & abandonment of offshore wells: Ensuring long-term well integrity and cost-efficiency. *Journal of Petroleum Science and Engineering*, *173*, 478-491. https://doi.org/https://doi.org/10.1016/j.petrol.2018.10.049
Wang, C., Chen, X., Wei, X., & Wang, R. (2017). Can nanosilica sol prevent oil well cement from strength retrogression under high temperature? *Construction and Building Materials*, *144*, 574-585. https://doi.org/https://doi.org/10.1016/j.conbuildmat.2017.03.221
Zhang, J. J. (2019). Chapter 2 - Rock physical and mechanical properties. In J. J. Zhang (Ed.), *Applied Petroleum Geomechanics* (pp. 29-83). Gulf Professional Publishing. https://doi.org/https://doi.org/10.1016/B978-0-12-814814-3.00002-2
Zheng, Y., Sun, D., Feng, Q., & Peng, Z. (2022). Nano-SiO2 modified basalt fiber for enhancing mechanical properties of oil well cement. *Colloids and Surfaces A: Physicochemical and Engineering Aspects*, *648*, 128900. https://doi.org/https://doi.org/10.1016/j.colsurfa.2022.128900